Imperial College London

Department of Mechanical Engineering
South Kensington, London, SW7 2AZ

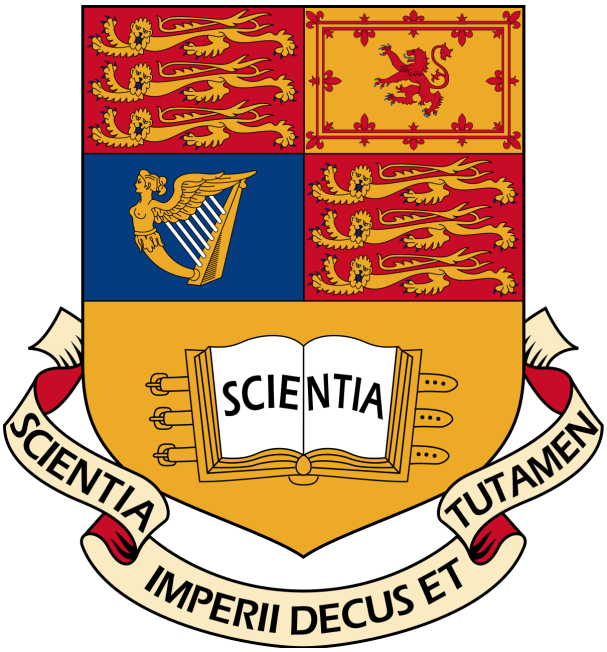

Rapidly Varying Open Channel Flow

Final Report
Master's Thesis

Author - Henry Hart
CID - 01190775
Supervisor - Dr. Peter Johnson
Date - 4th June 2020
Word Count - 11,998 (13,724 inc. listings)
Word Limit - 12,000

Abstract

This document is the Final Report detailing the work completed for the Individual Project element of the final year of the Mechanical Engineering Integrated Master's Degree at Imperial College.

The goal of the project is to advance understanding of rapidly varying open channel flow to an extent that the energetic transition length can be predicted accurately. This definition of transition is one where the flow becomes steady, having been rapidly varying in speed and geometry upstream of this transition. This project builds on work previously completed by two students, and will require further work to fully complete the goal.

This goal has been approached in two ways, which form the basis for the two objectives of the project. These are:

1. Create a statistical model for the flow.
2. Create an analytical model for the flow.

Both aims have been accomplished and are detailed herein. The accuracy of the models listed above is not considered suitable so as to consider the goal achieved by the author. The results achieved, however, form a sound basis for further work which may accomplish the goal of this project. In particular, the full analytical model derived for the flow in this project should predict the flow accurately if solved numerically in future work.

Acknowledgements

I would like to thank Dr. Peter Johnson for supporting this project throughout, and particularly for his support in the challenging circumstances following the impact of COVID-19 pandemic on the experimental elements of this project. Derivation of the solution of the governing simplified differential equation, as discussed in Section 3.3, was provided by Dr. Johnson and Dr. Jamie Jackson.

I would also like to thank Keith Blackney and Efi Bekiri for their help, guidance and company in the thermo-fluids laboratory.

Contents

1. Introduction

Open channel flows are an area of interest for engineers and have been for some time [1]. Rivers, canals and segmented pipe flows all rely on open channel flow theory for prediction of flow rate, speed and head loss [2].

This project is concerned with the transition of open channel flow from a tall, stagnant initial state to a shallower, steadily flowing channel state (see Figure 1.1).

While gradually varying flow is well theorised and understood, rapidly varying open channel flow is less well understood. There exist potential flow models [12] for the transition from gradually varying flow[1] to rapidly varying flow[2], for example flow encountering a sharp change in gradient. However, viscous theories to explain the transition from unsteady to steady Lagrangian[3] fluid particle height are not comprehensive. As a result, the factors influencing what will henceforth be known as the energetic transition length, or just transition length, are not well understood. This project aims to determine these factors and their effects using both an analytical approach (Section 3) and an experimentally derived statistical model (Section 4). The **goal** of this project is to be able to reliably predict transition length using known input parameters, and the project objectives set out in Section 1.2 are designed to achieve this goal. While the objectives have been completed, the accuracy of the results is not sufficient to have achieved the goal of the project. Significant progress, however, has been made and forms an elevated platform from which further work may be undertaken as set out in Section 6.2.

1.1 Project Overview

Due to previous work completed by Vasquez Calle [3], an experimental rig has already been built and is close to functional. This rig consists of a rectangular open channel Section

[1] A gradually varying flow particle experiences accelerating (gravitational & pressure) and decelerating (viscous) forces which are almost balanced.

[2] Rapidly varying flow is characterised by flow geometry causing viscous effects to be negligible.

[3] A Lagrangian framework follows a fluid particle as it moves through space.

between two reservoirs as shown in Figure 1.1. This rig allows a number of parameters to be varied and quantified as shown in Table 1.1. Previous work has focussed on varying flow rate, channel width, entry radius and channel slope in order to vary varying interpretations of the Froude and Reynolds number. This project investigates a number of additional variables, including a bump characteristic length as a literature review (see Section 2) suggests that this could affect transition length.

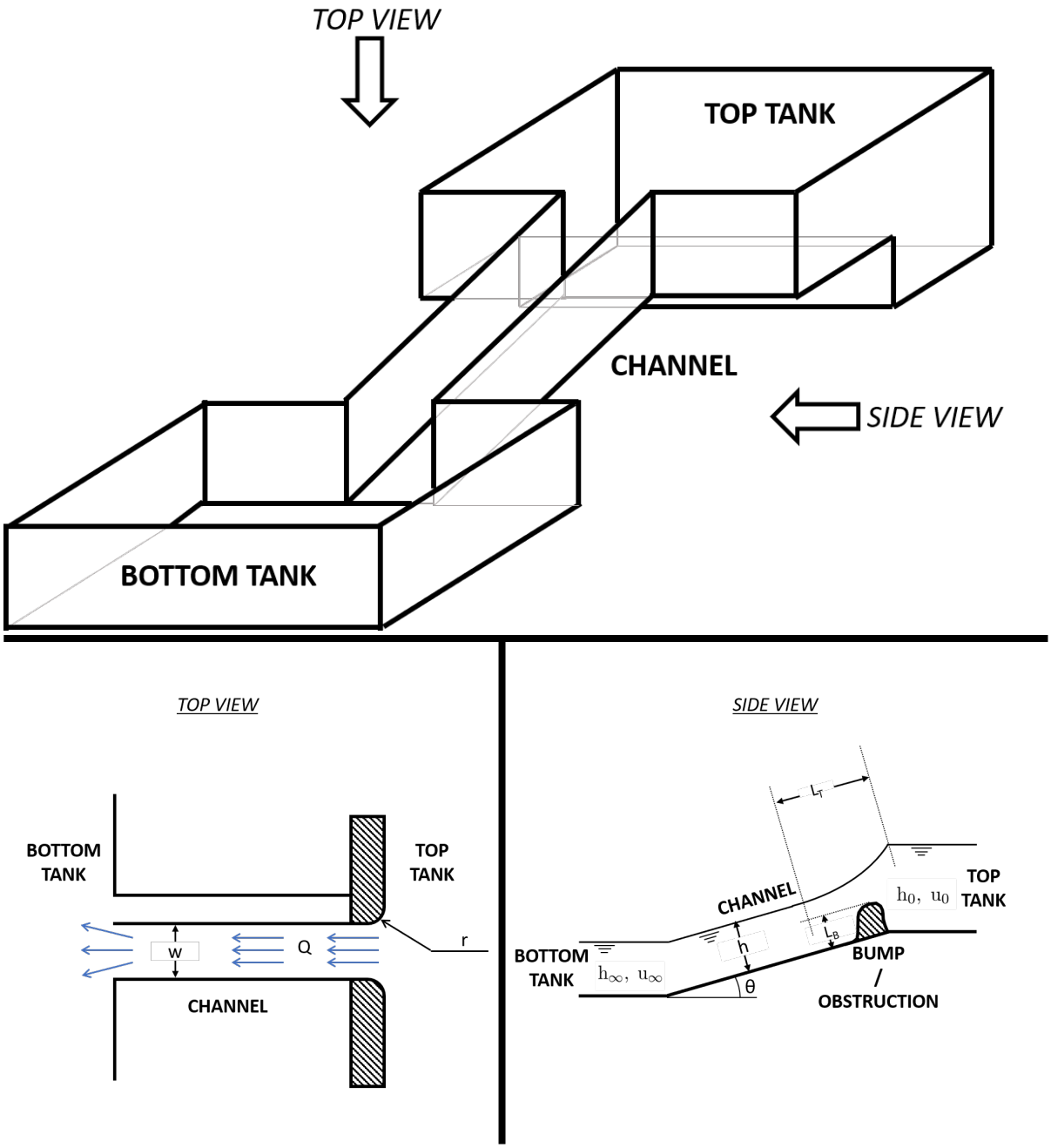

Figure 1.1: Schematic of Existing Rig [4];

Table 1.1: Parameters in Model [4];

Parameter	**Symbol Used (see Figure 1.1)**	**Units**
Independant		
Flow Rate	Q	$m^3\ s^{-1}$
Channel Width	w	m
Channel Entry Radius	r	m
Channel Slope	θ	non-dimensional
Bump Characteristic Length	L_B	m
Universal		
Gravity	g	$m\ s^{-2}$
Density	ρ	$kg\ m^{-3}$
Viscosity	μ	$kg\ m^{-1}\ s^{-1}$
Derived		
Froude	Fr_x (=$\frac{u^3 w}{gQ}$)	non-dimensional
Reynolds	Re (=$\frac{\rho u h}{\mu}$)	non-dimensional
Bulk Velocity	u (=$\frac{Q}{wh}$)	$m\ s^{-1}$
Measured		
Transition Length	L_t	m
Final Surface Height	h_∞	m
Beginning Surface Height	h_0	m

1.2 Objectives

Project objectives have been defined in the project plan report due near the beginning of this project. They are reproduced below to give context to the work detailed herein [4]:

1. Create parametric model for how transition length varies with other experimental parameters as detailed in Table 1.1 (see Section 4);
2. Investigate theoretical explanations for outcome (see Section 3);

Initially, more time was planned for experimental work in order to improve the model investigated in Section 4, however with access to the laboratory and equipment not possible after March 2020 due to the COVID-19 pandemic, more time was spent collaborating with supervisor Dr. Peter Johnson on analytical models for the flow, given in Section 3.

2. Literature Review

This literature review will aim to be brief and give an overview of relevant theories pertaining to this project. The concepts detailed herein are chosen so as to influence selection of parameters in the experimental phase of the project (Section 4).

Firstly, this review will summarise the two dominant theories of sloped channel flow: Gradually and Rapidly Varying Flow (Sections 2.1 $\&$ 2.2). Subsequently, an interesting outcome from previously completed work of students will be discussed [5] [3] (Section 2.3). Finally, literature regarding variable experimental parameters, as listed in Section 1.1, will be investigated to give insight into the expected experimental outcome (Sections 2.4 $\&$ 2.5).

2.1 Gradually Varying Flow Theory

Gradually Varying Flow theory (GVF) is the most basic theory that can be applied to sloped conduits carrying a fluid with a free surface. The assumptions of GVF are as follows [6]:

1. Steady flow
2. Non-uniform flow in channel
3. Gradual change in water depth
4. Friction is dominant

GVF relies on an analysis of specific energy of the flow as defined by Bakhmeteff [7] where V is the bulk velocity, y is the water height and z is the channel floor height:

$$E = \frac{V^2}{2g} + y + z \tag{2.1}$$

Figure 2.1 describes a control volume used for the analysis for GVF. EGL is the energy grade line and HGL is the hydraulic grade line. In this example of GVF, the EGL slopes downward due to the head loss associated with the flow. The 'rate' of head loss is described by the EGL slope S, and the addition of potential energy by the channel slope is described by

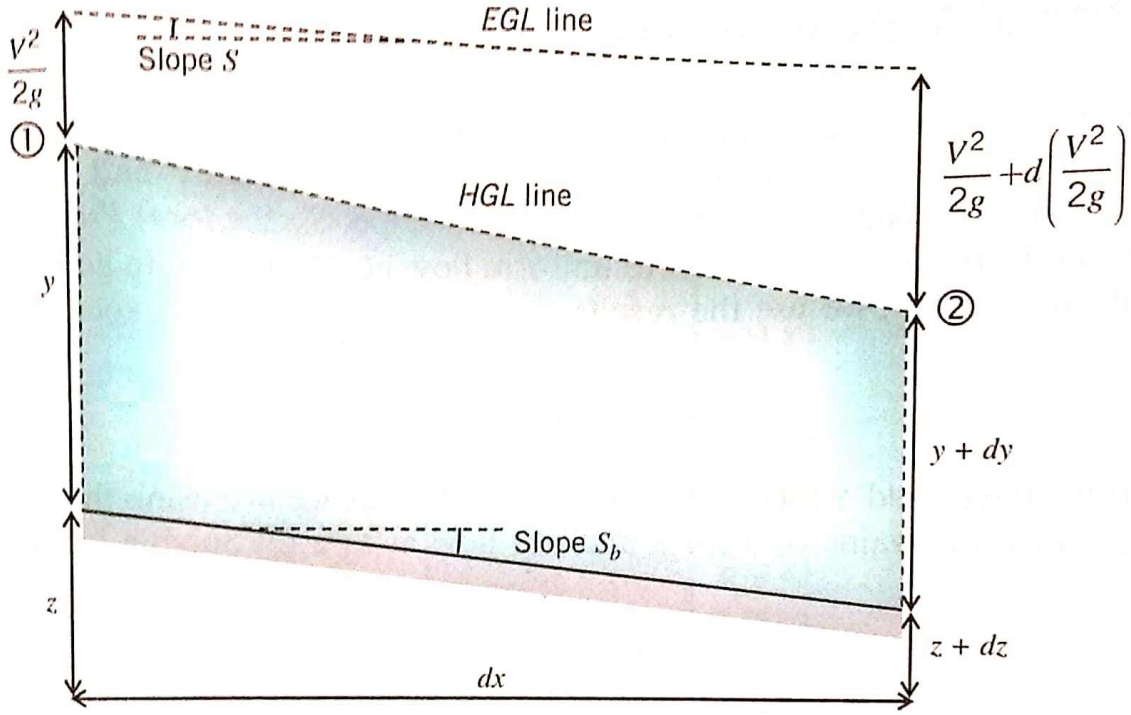

Figure 2.1: GVF Control Volume [6];

S_b. An energy balance leads to the energy Equation for GVF [6]:

$$\frac{dy}{dx} = \frac{S_b - S}{1 - Fr^2} \tag{2.2}$$

where the Froude number is defined as follows:

$$Fr = \sqrt{\frac{V^2}{y_h g}} \quad ; \qquad y_h = \frac{channel\,area}{free\,surface\,width} \tag{2.3}$$

Using the GVF energy, it is possible to estimate surface profiles by estimating the properties (right-hand side of Equation 2.2) at each point down the slope. Importantly, Equation 2.2 demonstrates the concept of criticality. This concept is the manifestation of the behaviour of GVF such that when the Froude number becomes larger or smaller than one, the slope of the free surface inverts. A sub-critical flow is one with a Froude number less than one, and super-critical otherwise.

2.2 Rapidly Varying Flow Theory

While GVF is a good theory for predicting flows on shallow slopes (i.e. rivers, canals and shallow conduits) it does not predict what happens when the flow experiences a rapid change

in channel geometry, whether that be as a result of a constriction, expansion or dramatic slope change [8]. Work done by Montes [8] calculates the surface profile of a rapidly varying flow using a potential flow approach. Necessarily therefore viscous effects are neglected, but this assumption produces accurate results because the dominant energy transition is from potential to kinetic in this scenario. Montes uses Ehrenburger's experimental results [9] to confirm his findings as shown in Figure 2.2. Andersen's work of 1975 also shows agreement

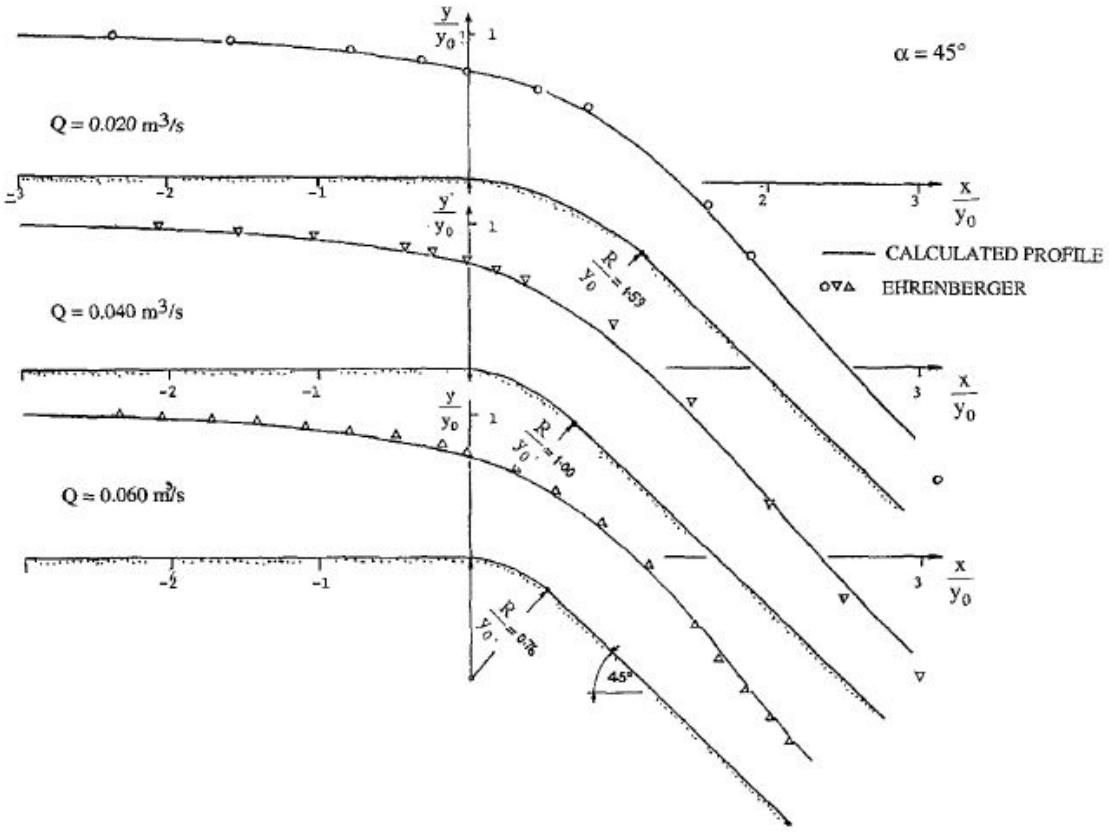

Figure 2.2: Montes' Potential Flow Prediction [8] and Ehrenburger's Experimental Results [9];

between a potential flow prediction and experimental results in the initial transition region [10]. While it is valuable to know that viscous effects are negligible as a sharp change in gradient is encountered, this is not exactly the region of interest for this project. In Section 2.3 a viscous theory of the constant slope transition will be examined.

2.3 Exponential Decay Model

This project is a continuation of work completed by Marta Vasquez Calle [3] and Daryl Pay [5]. In the original work, Vasquez Calle suggests a theory based on a model analogous to terminal velocity. In this model, the viscous friction is modelled to be proportional to the square of the bulk velocity of a fluid particle. This results implies a velocity profile as given below, where θ is the slope angle, m is the particle mass, x is the distance along the channel and C is a coefficient defining the viscosity:

$$V^2 = \frac{mgsin\theta}{C}(1 - e^{-\frac{2Cx}{m}}) \tag{2.4}$$

This formulation of the square of the velocity, when combined with the GVF energy Equation 2.2 implies an exponential decay for the height profile of the flow. Despite the numerous assumptions made to reach this output, Pay showed that an exponential fit is reasonably valid for his experimental data [5]. Figure 2.3 below shows a sample exponential fit from Pay's data set. This result implies that a higher 'drag coefficient' results in a smaller transition length.

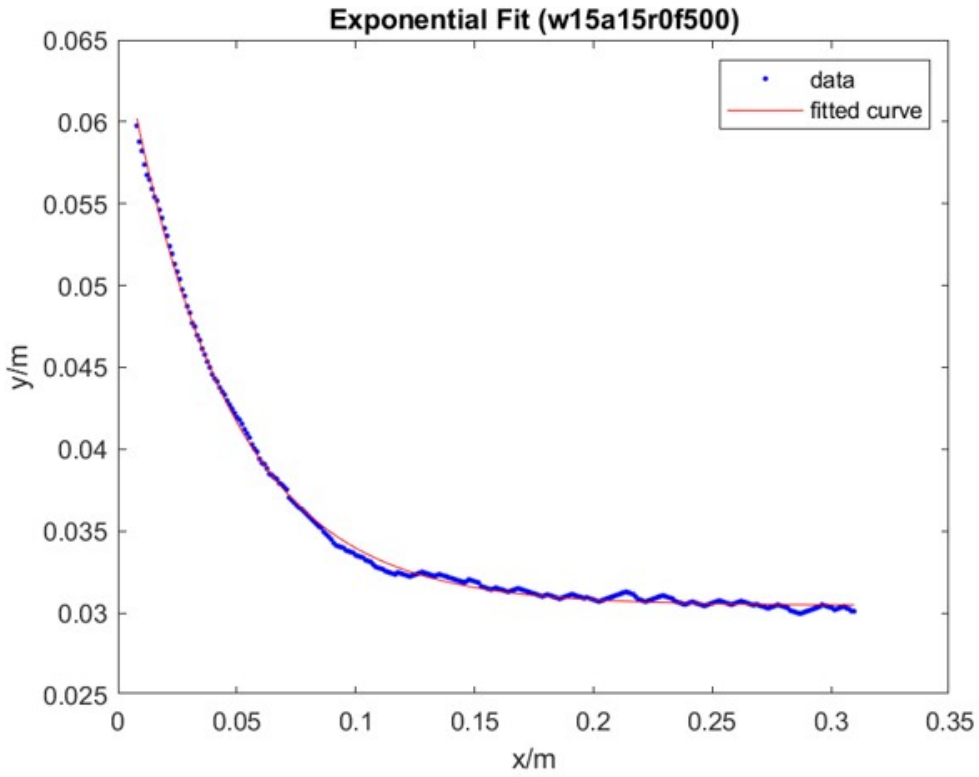

Figure 2.3: Sample Exponential Fit [5];

This raises the question of how to increase the 'drag coefficient'. One possible method would be to roughen the surfaces of the channel. Another would be to have a smaller flow rate; a

reduced flow would imply that a higher proportion of the fluid is in contact with the surfaces. Pay's work did not find a strong correlation between the Reynolds number (a proxy for flow rate) and exponent magnitude (a proxy for transition length) [5].

While certainly this theory is cogent, it would be interesting to compare it to one where a constant 'drag coefficient' is not assumed. As the fluid section, or particle, becomes more flattened, the proportion of the fluid in contact with surfaces will change and so one would expect a variable 'drag coefficient'. This analysis has been completed in Section 3.

2.4 Entry Geometry

Entry geometry is one of the variables which may have an effect on transition length. Indeed, having a 'sharper' entry geometry would certainly reduce the length to transition to turbulence and so could increase the drag, which could in turn reduce the energetic transition length (see Section 2.3).

Unsurprisingly, contractions and expansions in channel geometry are not completely efficient in energy terms and so cause a head loss on the flow. Formica investigated a number of expansion and contraction profiles in open channel flows ranging from sharp cornered entry to a long smooth transition as shown in Figure 2.4 [11]. The geometries labelled I to IV have loss coefficients of 0.06 to 0.1. The geometries labelled 1 to 8 have loss coefficients of 0.44 to 0.82. Loss coefficients for expansion and contraction, ϵ and K are defined as follows:

$$\Delta E = \epsilon \frac{(V_{in} - V_{out})^2}{2g} \quad ; \quad \Delta E = K \frac{V_{in}^2}{2g} \tag{2.5}$$

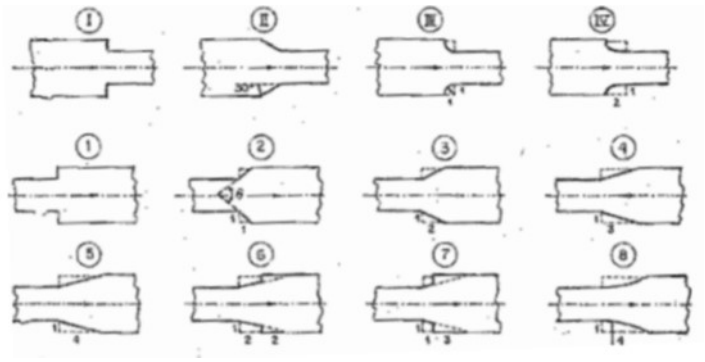

Figure 2.4: Tested geometries [11];

2.5 Obstructions

Obstructions, in a similar manner to variable entry geometry, can alter the behaviour of flow downstream. Firstly, an obstruction will be a source of head loss in a viscous flow due to the acceleration associated with the contraction. Additionally, a contraction in the flow before Lagrangian steadiness is achieved could cause more rapid collapse of the flow. Work done by Dias and Vanden-Broeck suggests that obstructions can cause a flow to transition from sub-critical to super-critical, even when the flow is modelled as potential flow [12]. As can be seen from Figures 2.5 and 2.6, the constriction of the flow over the obstruction acts to permanently collapse the flow to a height not dissimilar to that at the apex of the obstruction. This suggests that a flow can be caused to transition earlier if an obstruction is placed at the mouth of the channel entry. This study also suggests that the optimal height for the obstruction is one where the local flow height over the obstruction is equal to the transitioned height.

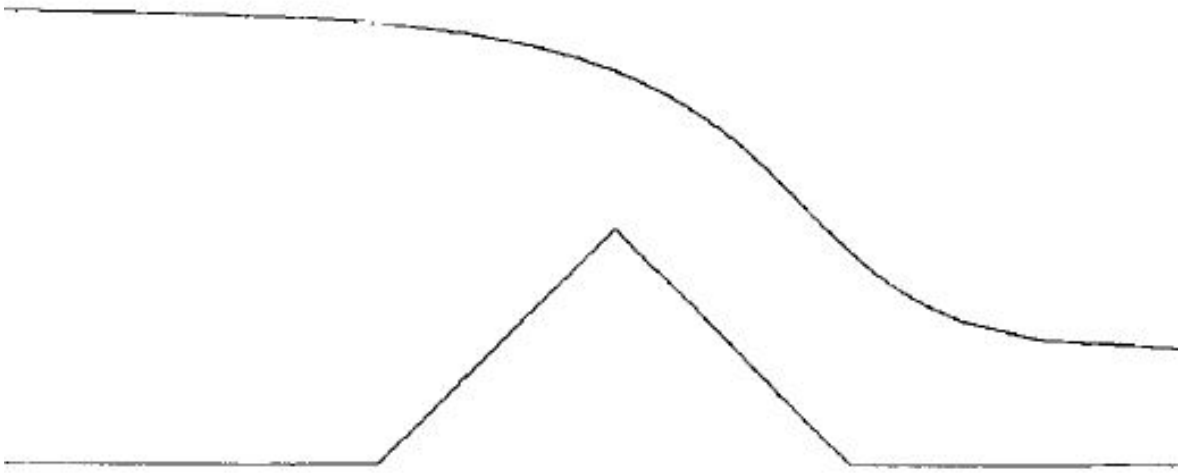

Figure 2.5: Potential Flow Over a Triangular Obstruction [12];

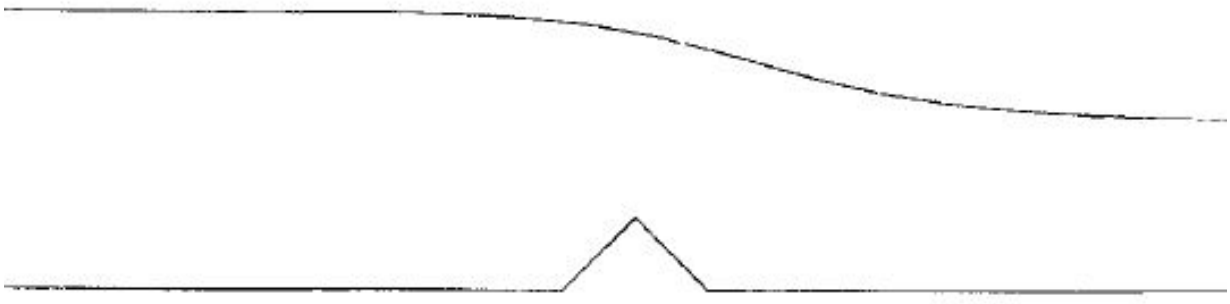

Figure 2.6: Potential Flow Over a Triangular Obstruction [12];

3. Analytical Model

3.1 Differential Equation

This Section derives a bulk flow analytical model for the flow considered herein. The governing Equation to begin the derivation will be the Reynolds Averaged Navier-Stokes Equations [13] (Equation 3.1), where all terms should be considered locally time-averaged. Assumptions are listed in Table 3.1.

$$\cancel{\frac{\partial}{\partial t}}^{\text{(i)}} u_i + u_j \frac{\partial u_i}{\partial x_j} = -\frac{1}{\rho}\frac{\partial p}{\partial x_i} + g_i + \frac{1}{\rho}\nabla \cdot \underline{\underline{\tau}} \tag{3.1}$$

From here it is convenient to resolve the Equations into the x, y and z directions as defined by Figure 3.1. This is a Cartesian coordinate system.

$$u\frac{\partial u}{\partial x} + v\cancel{\frac{\partial u}{\partial y}}^{\text{(iv)}} + w\cancel{\frac{\partial u}{\partial z}}^{\text{(iii)}} = -\frac{1}{\rho}\frac{\partial p}{\partial x} + g\sin\theta + \hat{\imath}\cdot\left(\frac{1}{\rho}\nabla\cdot\underline{\underline{\tau}}\right) \tag{3.2}$$

$$u\frac{\partial v}{\partial x} + v\frac{\partial v}{\partial y} + w\cancel{\frac{\partial v}{\partial z}}^{\text{(iii)}} = -\frac{1}{\rho}\frac{\partial p}{\partial y} - g\cos\theta + \hat{\jmath}\cdot\left(\frac{1}{\rho}\nabla\cdot\underline{\underline{\tau}}\right) \tag{3.3}$$

$$u\cancel{\frac{\partial w}{\partial x}}^{\text{(iii)}} + v\cancel{\frac{\partial w}{\partial y}}^{\text{(iii)}} + w\cancel{\frac{\partial w}{\partial z}}^{\text{(iii)}} = -\frac{1}{\rho}\frac{\partial p}{\partial z} + \cancel{g_z}^{\text{(ii)}} + \cancel{\hat{k}\cdot\left(\frac{1}{\rho}\nabla\cdot\underline{\underline{\tau}}\right)}^{\text{(iii)}} \tag{3.4}$$

Table 3.1: Assumptions for simplification;

Assignment	Assumption
(i)	Globally steady flow[1]: $\frac{\partial \vec{u}}{\partial t} = \vec{0}$
(ii)	No body force in z-direction: $g_z = 0$
(iii)	Negligible z-direction time averaged velocity: $w = 0$
(iv)	Bulk velocity model: $\frac{\partial u}{\partial y} = 0$

[1] This analysis allows for locally unsteady turbulent fluctuations whose effect is accounted for in the friction term.

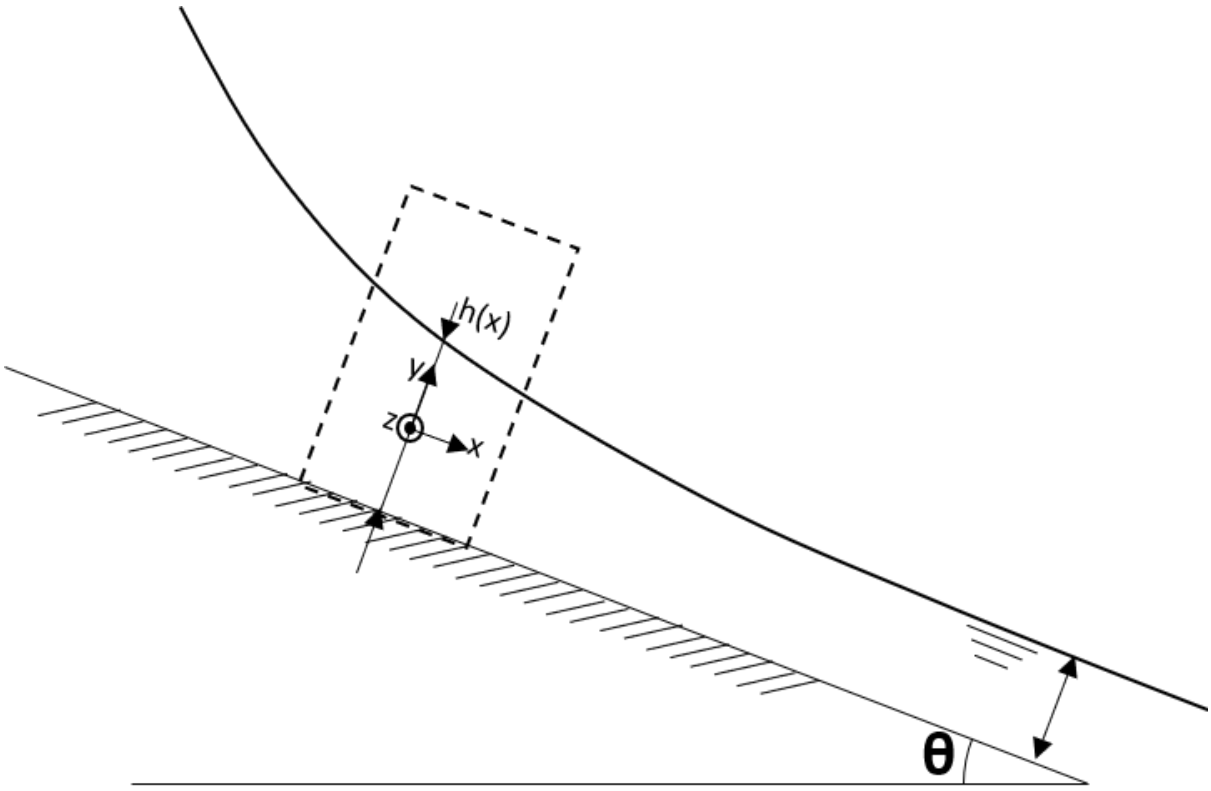

Figure 3.1: Analytical control volume;

3.1.1 Pressure Model

On the free surface, the velocity of the fluid must be parallel to the free surface. Likewise, on the floor of the channel, the flow must be parallel to the impermeable floor. In reality, there is also a no-slip condition on the floor of the channel; for now let us assume a parallel velocity on the floor which may be set to zero.

Figure 3.2 shows the flow through a short[2] control volume. Since the y-direction velocity smoothly turns from non-zero at the free-surface to zero at the floor, it is not unreasonable to assume that this relationship is linear, as shown in Equation 3.5.

$$v(x,y) = u(x,y)\frac{y}{h(x)}\frac{dh}{dx} \tag{3.5}$$

Recall the y-direction RANS equation, but repeated here in the full 2-dimensional form (i.e. zero z-direction velocity is implied):

$$u\frac{\partial v}{\partial x} + v\frac{\partial v}{\partial y} = -\frac{1}{\rho}\frac{\partial p}{\partial y} - g\cos\theta + \hat{\jmath}\cdot\left(\frac{1}{\rho}\nabla\cdot\underline{\underline{\tau}}\right) \tag{3.6}$$

Continuity applies, allowing the x-direction and y-direction gradients to be related to one

[2] 'Short' is meant to imply that the small dimension is the x-direction.

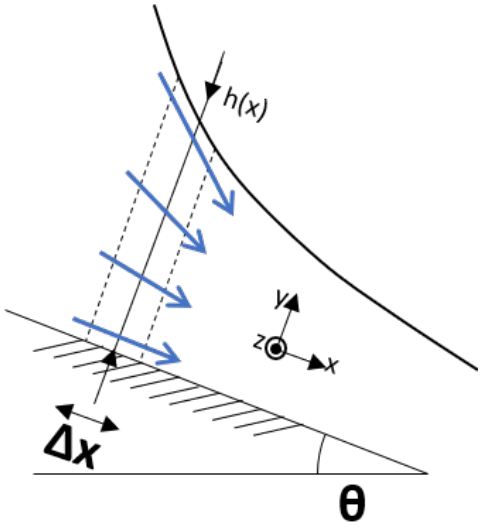

Figure 3.2: Short 2-dimensional control volume;

another:

$$\frac{\partial v}{\partial y} = -\frac{\partial u}{\partial x} \tag{3.7}$$

Combining Equation 3.6 with Equations 3.5 and 3.7 gives the following:

$$u\frac{\partial}{\partial x}\left(u\frac{y}{h}\frac{dh}{dx}\right) - u\frac{y}{h}\frac{dh}{dx}\frac{\partial u}{\partial x} = -\frac{1}{\rho}\frac{\partial p}{\partial y} - g\cos\theta - C_f\frac{v^2}{R} \tag{3.8}$$

The y-direction friction drag has been modelled as follows:

$$\hat{\jmath}\cdot\left(\frac{1}{\rho}\nabla\cdot\underline{\underline{\tau}}\right) = -C_f\frac{v^2}{R} \;\;;\;\; R = 2h(x) + w \tag{3.9}$$

Expanding the first term gives the following:

$$u\left(u\frac{y}{h}\frac{d^2h}{dx^2} + uy\frac{dh}{dx}\frac{d}{dx}\left(\frac{1}{h}\right) + \cancel{\frac{y}{h}\frac{dh}{dx}\frac{\partial u}{\partial x}}\right) - \cancel{u\frac{y}{h}\frac{dh}{dx}\frac{\partial u}{\partial x}} = -\frac{1}{\rho}\frac{\partial p}{\partial y} - g\cos\theta - C_f\frac{v^2}{R} \tag{3.10}$$

Substituting in Equation 3.5:

$$yu^2\frac{1}{h}\frac{d^2h}{dx^2} + yu^2\frac{dh}{dx}\frac{d}{dx}\left(\frac{1}{h}\right) = -\frac{1}{\rho}\frac{\partial p}{\partial y} - g\cos\theta - C_f\frac{u^2}{R}\left(\frac{y}{h}\frac{dh}{dx}\right)^2 \tag{3.11}$$

Now relations defining flow rate and hydraulic radius are used to express Equation 3.11 in

terms of h:

$$y\left(\frac{Q}{wh}\right)^2\left(\frac{1}{h}\frac{d^2h}{dx^2}+\frac{dh}{dx}\frac{d}{dx}\left(\frac{1}{h}\right)+\frac{C_f\cdot y}{h^2(2h+w)}\left(\frac{dh}{dx}\right)^2\right)=-\frac{1}{\rho}\frac{\partial p}{\partial y}-g\cos\theta \tag{3.12}$$

$$y\left(\frac{Q}{wh}\right)^2\left(\frac{1}{h}\frac{d^2h}{dx^2}-\frac{1}{h^2}\left(\frac{dh}{dx}\right)^2+\frac{C_f\cdot y}{h^2(2h+w)}\left(\frac{dh}{dx}\right)^2\right)=-\frac{1}{\rho}\frac{\partial p}{\partial y}-g\cos\theta \tag{3.13}$$

[3]

Rearranging:

$$\frac{1}{\rho}\frac{\partial p}{\partial y}=-g\cos\theta-\frac{y}{h}\left(\frac{Q}{wh}\right)^2\left(\frac{d^2h}{dx^2}+\frac{1}{h}\left(\frac{dh}{dx}\right)^2\left(\frac{C_f\cdot y}{2h+w}-1\right)\right) \tag{3.14}$$

Integrating:

$$\frac{1}{\rho}p(x,y)=\int\left(-g\cos\theta-\frac{y}{h}\left(\frac{Q}{wh}\right)^2\left(\frac{d^2h}{dx^2}+\frac{1}{h}\left(\frac{dh}{dx}\right)^2\left(\frac{C_f\cdot y}{2h+w}-1\right)\right)\right)\partial y \tag{3.15}$$

$$=-gy\cos\theta-\frac{y^2}{2h}\left(\frac{Q}{wh}\right)^2\left(\frac{d^2h}{dx^2}\right)-\frac{y^3}{3h^2}\left(\frac{Q}{wh}\right)^2\left(\frac{dh}{dx}\right)^2\frac{C_f}{2h+w}+\frac{y^2}{2h^2}\left(\frac{Q}{wh}\right)^2\left(\frac{dh}{dx}\right)^2+f(x) \tag{3.16}$$

Now, defining the origin at the centre of tall, thin control volume as shown by Figure 3.1, the pressure can be found in terms of height ($h(x)$) and y using the boundary condition of zero relative pressure on the free surface.

$$p(x,y=\frac{1}{2}h(x))=0 \tag{3.17}$$

$$\begin{aligned}\implies \frac{1}{\rho}p(x,y)=&-g\cos\theta\left(y-\frac{1}{2}h\right)-\left(\frac{Q}{wh}\right)^2\left(\frac{d^2h}{dx^2}\right)\left(\frac{y^2}{2h}-\frac{h}{8}\right)\\&-\left(\frac{Q}{wh}\right)^2\left(\frac{dh}{dx}\right)^2\frac{C_f}{2h+w}\left(\frac{y^3}{3h^2}-\frac{h}{24}\right)+\left(\frac{Q}{wh}\right)^2\left(\frac{dh}{dx}\right)^2\left(\frac{y^2}{2h^2}-\frac{1}{8}\right)\end{aligned} \tag{3.18}$$

[3] $\frac{d}{dx}\left(\frac{1}{h}\right)=-\frac{1}{h^2}\frac{dh}{dx}$

Now the 'bulk pressure' used henceforth is defined as follows.

$$\overline{p}(x) = \frac{\int_{-\frac{1}{2}h}^{\frac{1}{2}h} p(x,y)dy}{\int_{-\frac{1}{2}h}^{\frac{1}{2}h} dy} \tag{3.19}$$

$$\implies \frac{1}{\rho}\overline{p}(x) = \underbrace{\frac{h}{2}g\cos\theta}_{\text{Hydrostatic}} + \frac{1}{24}\left(\frac{Q}{wh}\right)^2 \left(\underbrace{h\frac{d^2h}{dx^2}}_{\text{Curvature}} + \left(\frac{dh}{dx}\right)^2 \left(\underbrace{\frac{C_f \cdot h}{2h+w}}_{Viscous} - \underbrace{1}_{Advective} \right) \right) \tag{3.20}$$

This total bulk pressure model can then be approximated in three ways:

Full Bulk Pressure Model

In this model, none of the terms from Equation 3.20 are discounted.

$$\frac{1}{\rho}\overline{p}(x) = \underbrace{\frac{h}{2}g\cos\theta}_{\text{Hydrostatic}} + \frac{1}{24}\left(\frac{Q}{wh}\right)^2 \left(\underbrace{h\frac{d^2h}{dx^2}}_{\text{Curvature}} + \left(\frac{dh}{dx}\right)^2 \left(\underbrace{\frac{C_f \cdot h}{2h+w}}_{Viscous} - \underbrace{1}_{Advective} \right) \right) \tag{3.21}$$

Order of Magnitude Approximation

In this approximation, the curvature and viscous terms in Equation 3.20 are discounted.

The curvature term can be neglected when the radius of curvature of the flow is small, and so this approximation is only valid for smooth variations in flow slope.

The viscous term can be neglected on the basis of its insignificance in comparison to the advective term. Since the width is positive, the largest magnitude that the dimensionless viscous term could have is as follows:

$$\min\left[\frac{C_f \cdot h}{2h+w}\right] = \lim_{w\to 0}\frac{C_f \cdot h}{2h+w} = \frac{1}{2}\cdot C_f \tag{3.22}$$

Recall the definition of the friction model used:

$$C_f = \hat{\jmath}\cdot\left(\frac{1}{\rho}\nabla\cdot\underline{\underline{\tau}}\right)\frac{R}{v^2} \tag{3.23}$$

The friction coefficient may be approximated for laminar boundary layers using the Blasius solution [14], shown in Equation 3.24, or for turbulent boundary layers using Prantl's

one-seventh-power law [15], shown in Equation 3.25.

$$C_{f,\text{Blasius}} = 2 \cdot \frac{0.664}{\sqrt{Re_x}} \tag{3.24}$$

$$C_{f,\text{Prantl}} = 2 \cdot \frac{0.027}{Re_x^{1/7}} \tag{3.25}$$

Note that the formulations of C_f used herein differ by a factor of 2 from those typically seen in the literature due to the definition of C_f used throughout this report.

Using the characteristic quantities shown in Equation 3.26, the orders of Blasius and Prantl C_f can be approximated as shown in Equation 3.27.

$$\begin{aligned} \mathcal{O}(u) &= 1 \text{ ms}^{-1} \\ \mathcal{O}(x) &= 1 \ m \\ \mathcal{O}(\nu) &= 10^{-6} \text{ m}^2\text{s}^{-1} \\ \implies \mathcal{O}(Re_x) &= 10^6 \end{aligned} \tag{3.26}$$

$$\begin{aligned} \mathcal{O}(C_{f,\text{Blasius}}) &= 10^{-3} \\ \mathcal{O}(C_{f,\text{Prantl}}) &= 10^{-2} \end{aligned} \tag{3.27}$$

These values align with the order of the similarly defined Moody friction factor for high Reynolds number [16].

Therefore the error due to neglecting the viscous term in the pressure model (i.e. y-direction friction) is approximately 1%.

Neglecting the curvature and viscous terms yields the following model for bulk pressure:

$$\frac{1}{\rho}\overline{p}(x) = \underbrace{\frac{h}{2} g \cos\theta}_{\text{Hydrostatic}} \underbrace{- \frac{1}{24}\left(\frac{Q}{wh}\right)^2 \left(\frac{dh}{dx}\right)^2}_{Advective} \tag{3.28}$$

Hydrostatic Model

Rearranging Equation 3.28, the dimensionless bulk pressure for small $\frac{d^2h}{dx^2}$ and small C_f can be expressed as follows:

$$\frac{\overline{p}(x)}{\rho g h} = \frac{1}{2}\cos\theta - \frac{1}{24}\frac{Q^2}{g w^2 h^3}\left(\frac{dh}{dx}\right)^2 \tag{3.29}$$

$$= \frac{1}{2}\cos\theta - \frac{1}{24}\frac{u^3 w}{gQ}\left(\frac{dh}{dx}\right)^2 \tag{3.30}$$

Now the local Froude number is defined as follows:

$$Fr_x \equiv \frac{u^3 w}{gQ} \tag{3.31}$$

$$\implies \frac{\overline{p}(x)}{\rho g h} = \underbrace{\frac{1}{2}\cos\theta}_{Hydrostatic} \underbrace{- \frac{1}{24} Fr_x \left(\frac{dh}{dx}\right)^2}_{Advective} \tag{3.32}$$

Now the relative magnitude of the hydrostatic and advective terms may be compared for different Froude numbers and slopes. For small slopes and Froude numbers, the advective terms may be neglected giving the hydrostatic approximation for bulk pressure. Note that this expression also relies on previous assumptions including low $\frac{d^2h}{dx^2}$ and C_f:

$$\frac{1}{\rho}\overline{p}(x) = \frac{h}{2} g \cos\theta \tag{3.33}$$

A flowchart outlining the assumptions used to arrive at various forms of the y-direction Equation and pressure models is shown in Figure 3.3.

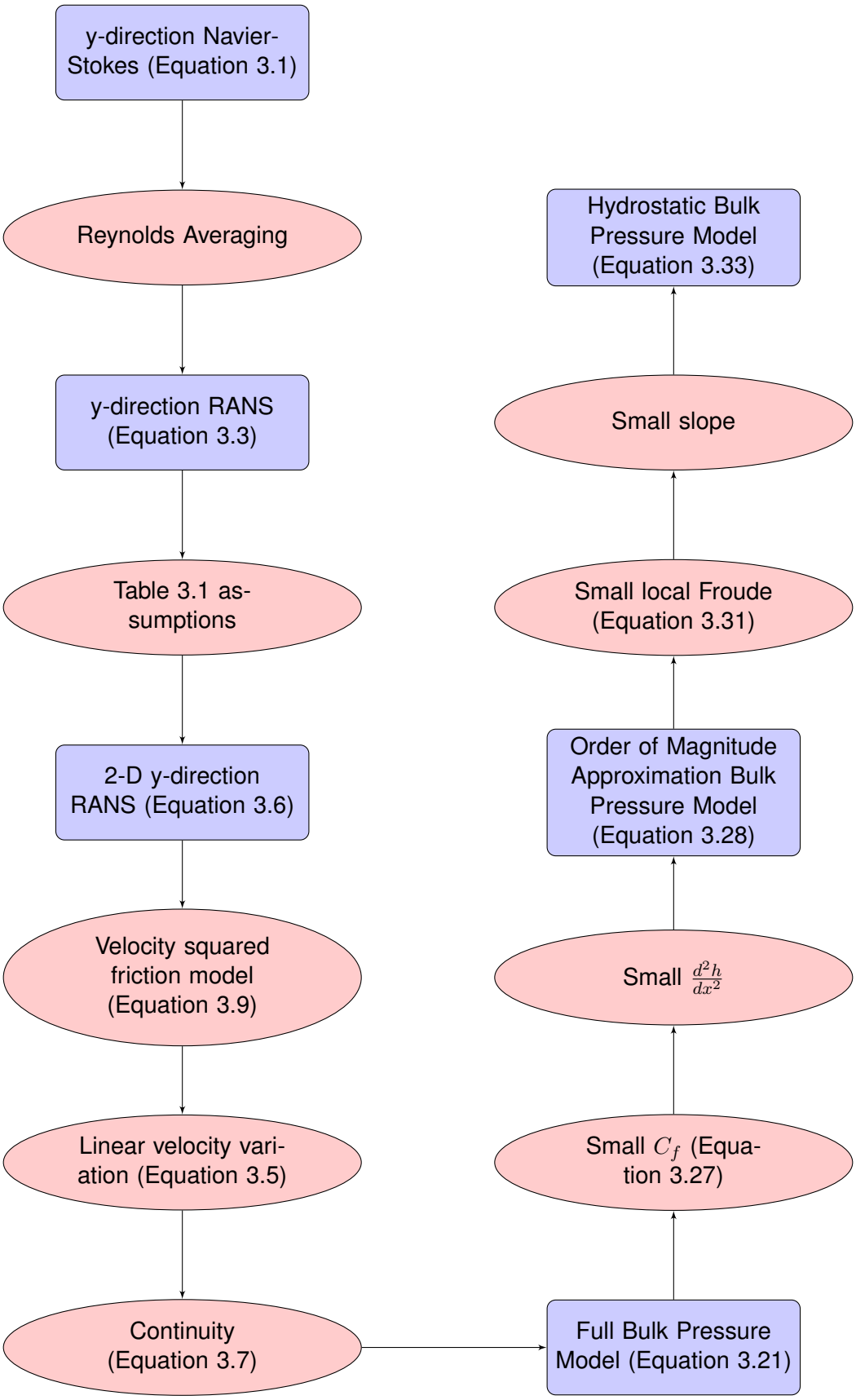

Figure 3.3: Pressure Models Flow Chart;

3.2 Velocity Equation

The simplified x-direction Equation with assumptions of bulk pressure and velocity is given below:

$$u\frac{\partial u}{\partial x} = -\frac{1}{\rho}\frac{\partial p}{\partial x} + g\sin\theta + \hat{\imath}\cdot\left(\frac{1}{\rho}\nabla\cdot\underline{\underline{\tau}}\right) \tag{3.34}$$

Again, the friction term is modelled as proportional to the square of the velocity as per Equation 3.9:

$$\hat{\imath}\cdot\left(\frac{1}{\rho}\nabla\cdot\underline{\underline{\tau}}\right) = -C_f\frac{u^2}{R} \;\;;\;\; R = 2h(x) + w \tag{3.35}$$

$$u\frac{\partial u}{\partial x} = -\frac{1}{\rho}\frac{\partial p}{\partial x} + g\sin\theta - C_f\frac{u^2}{2h+w} \tag{3.36}$$

Note that Equation 3.34 is also solved by substituting the simpler terminal velocity model given in Section 2.3 as follows:

$$u\frac{\partial u}{\partial x} = \frac{1}{2}\frac{\partial u^2}{\partial x} \;\;;\;\; u^2 = V^2 = \frac{mg}{C}\sin\theta\left(1 - e^{\frac{2Cx}{m}}\right) \;\;;\;\; \hat{\imath}\cdot\left(\frac{1}{\rho}\nabla\cdot\underline{\underline{\tau}}\right) = -\frac{C}{m}V^2 \;\;;\;\; -\frac{1}{\rho}\frac{\partial p}{\partial x} = 0 \tag{3.37}$$

The exponential model for this flow shall not be considered in this Section henceforth as it neglects the effects of pressure and variable hydraulic radius.

3.2.1 ODE in h

Using the definition of bulk flow rate given in Equation 3.38, Equation 3.36 can be expressed in terms of the surface height, h, as shown in Equation 3.39:

$$u = \frac{Q}{wh} \tag{3.38}$$

$$-\frac{1}{h}\left(\frac{Q}{wh}\right)^2\frac{dh}{dx} = -\frac{1}{\rho}\frac{d\overline{p}}{dx} + g\sin\theta - C_f\left(\frac{Q}{wh}\right)^2\frac{1}{2h+w} \tag{3.39}$$

Equation 3.39 is an ordinary differential Equation in h and $\overline{p}$ with constant coefficients. Section 3.1.1 derived three formulations for the bulk pressure in terms of h, each with more restrictive assumptions than the last. This means that the surface height can be formulated as an ordinary differential Equation in h using Equations 3.39 and 3.21 (or a simpler bulk

pressure model). This ODE may then be solved using numerical or analytical techniques. One such analysis is given in Section 3.2.2.

3.2.2 Hydrostatic Analysis

As discussed in Section 3.1.1, a hydrostatic model for bulk pressure may be assumed when the assumptions listed in Figure 3.3 are satisfied. Substituting the hydrostatic bulk pressure model (Equation 3.33) into Equation 3.36 gives an ordinary differential Equation in u:

$$u\frac{du}{dx} + \frac{gQ\cos\theta}{2w}\frac{d}{dx}(\frac{1}{u}) = g\sin\theta - C_f\frac{u^3}{\frac{2Q}{w} + wu} \tag{3.40}$$

In this, the simplified Equation for the transport of bulk velocity $u(x)$, there are $n = 8$ (u, x, g, Q, w, θ, C_f & u_{ref}) independent quantities and $r = 2$ independent dimensions (length and time). Note that mass has been eliminated. Note also that u_{ref} does not appear in Equation 3.40, but it is useful as a reference for formation of dimensionless quantities. The chosen $n - r = 6$ dimensionless quantities are given below.

$$u^\star = \frac{u}{u_{ref}} \;\; ; \;\; x^\star = \frac{x}{h_{ref}} = \frac{xu_{refw}}{Q} \;\; ; \;\; Fr = \frac{u_{ref}^3 w}{gQ} \;\; ; \;\; \theta \;\; ; \;\; C_f \;\; ; \;\; w^\star = 1 + \frac{w^2 u_{ref}}{2Q} \tag{3.41}$$

These dimensionless parameters allow the Equation to be written in the following form.

$$\frac{\mathrm{d}}{\mathrm{d}x^\star}(Fr\cdot u^{\star 2} + u^{\star -1}\cos\theta) = 2\sin\theta - C_f\cdot Fr\frac{u^{\star 3}}{w^\star} \tag{3.42}$$

3.3 Differential Equation Solution

The differential Equation derived in Section 3.2 can be analytically solved to give dimensionless stream-wise distance as a function of dimensionless bulk velocity. The derivation of this solution is given in Appendix A. The derivation was provided by the project's supervisor, Dr. Peter Johnson, and Dr. Jamie Jackson.

$$x^\star = 2\sin\theta\left\{y + \frac{(p^3-q^3)}{6q^2}\left[-2\log(y-q) + \log\left(y^2+qy+q^2\right) + 2\sqrt{3}\arctan\left(\frac{2y+q}{q^2\sqrt{3}}\right)\right] + K\right\} \tag{3.43}$$

In this equation, y, p and q are derived quantities as given below:

$$y = \frac{1}{u^\star} = \frac{u_{ref}}{u} = \frac{h}{h_{ref}} \; ; \; p = \sqrt[3]{\frac{2Fr}{\cos\theta}} \; ; \; q = \sqrt[3]{\frac{FrC_f}{w^\star\cdot 2\sin\theta}} \tag{3.44}$$

By definition of fully developed flow used in this project, the LHS of Equation 3.42 must approach 0 as the flow travels downstream. Clearly then, from the definition of y and q, the fully developed dimensionless height can be expressed as follows:

$$y_\infty = q = \frac{h_\infty}{h_{ref}} \tag{3.45}$$

This means that q, and therefore C_f can be found from the ratio of fully developed height and reference height. This then allows p to be found. While it has been convenient up until now to keep reference height and velocity, h_{ref} and u_{ref}, undefined, it is now appropriate to define then as the channel mouth quantities. This allows the entrance and fully developed dimensionless distances to be found from Equation 3.43 as follows:

$$x_0{}^\star = x^\star \left(y = y_0 = 1\right) \tag{3.46}$$

Given that full transition occurs only asymptotically, it is convenient to define transition length at 105% of fully developed height:

$$x_T{}^\star = x^\star \left(y = 1.05 * y_\infty = 1.05 * q\right) \tag{3.47}$$

This allows the *theoretical* transition length according to the analysis herein (Section 3) to be calculated as follows:

$$L_T = h_0 \left(x_T{}^\star - x_0{}^\star\right) \tag{3.48}$$

Because the reference quantities have been defined at the channel mouth, theoretical transition length is a function of q and h_0 only, albeit a complex one. These parameters can be determined from experimental data. Comparison of this formulation of transition length and measured transition length for the collected experimental data is given in Section 5.

4. Experimental Phase

4.1 First Phase: Exploratory Experiments

A number of initial experiments were run to test some original ideas. These have been mostly qualitative and have served their main purpose of inspiring discussion of the physics at regular student-supervisor meetings. Additionally, failed experiments have helped to rule out certain proposed models for the flow. Details of each exploratory experiment are given in this section.

4.1.1 Bottom Weir

This experiment involves placing a weir at the entry to the channel. It was thought that this restriction would force the flow to accelerate and therefore collapse to a steady state sooner. This idea was backed by the potential flow simulations described in Section 2.5. This hypothesis did not hold in reality as can be seen in Figure 4.1 compared to the base case, Figure 4.2.

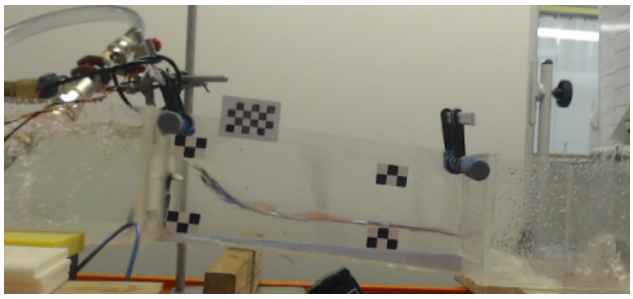

Figure 4.1: Flow with Bottom Weir;

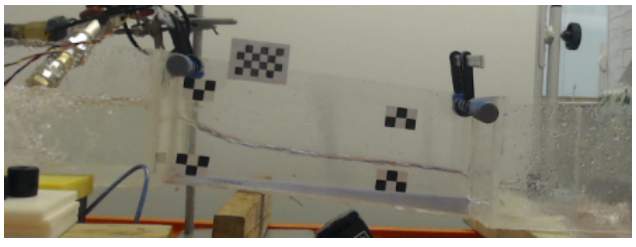

Figure 4.2: Base Case Flow;

While the transition slope is steeper in the modified experiment, the actual distance to transition is not significantly different. It is also notable that there is turbulent separation at the top of the sharp corner created by the weir.

4.1.2 Top Weir

While the experiment in Section 4.1.1 involved using a weir at the bottom of the entry flow, this experiment tests using a weir protruding into the flow from the top. While this method successfully flattened the flow curve out on average, there were a number of issues identified.

1. The flow was unsteady at entry due to the 3D entry geometry created by the top weir. This issue is easily resolved by integrating the weir with the vertical entry radii.
2. This method only works if you know the final developed height of the flow. This means that this method is not appropriate for inclusion in the final non-dimensional model.

The flow is shown in Figure 4.3.

Figure 4.3: Flow with Top Weir;

4.1.3 Downstream Constriction

The downstream constriction experiment involves restricting the section of the channel far downstream of entry in order to 'pre-accelerate' the flow relative to it's steady state viscous drag. The idea comes from Section 2.3 where it is implied that a 'drag coefficient' which is lower during transition could expedite the transition time and therefore length. Initial experiments have demonstrated a flattening of the flow, as in Figure 4.4, and this could be interpreted as a pre-acceleration.

4.1.4 Walls

As with other ideas for flow control, the placing of thin walls into the body of the flow seeks to alter the effective drag coefficient of the flow and so effect the transition length. This was

Figure 4.4: Flow with Downstream Constriction;

achieved by cementing thin plastic lamination sheets to laser cut acrylic spacers. While this proved a more rigid structure than previously attempted to achieve such a mid-flow wall arrangement, the sheets continued to respond somewhat dynamically to the flow, especially at high flow rates. This can be seen in Figure 4.5. The response of the flexible walls causes differing flow rates and or height profiles in the sub-channel.

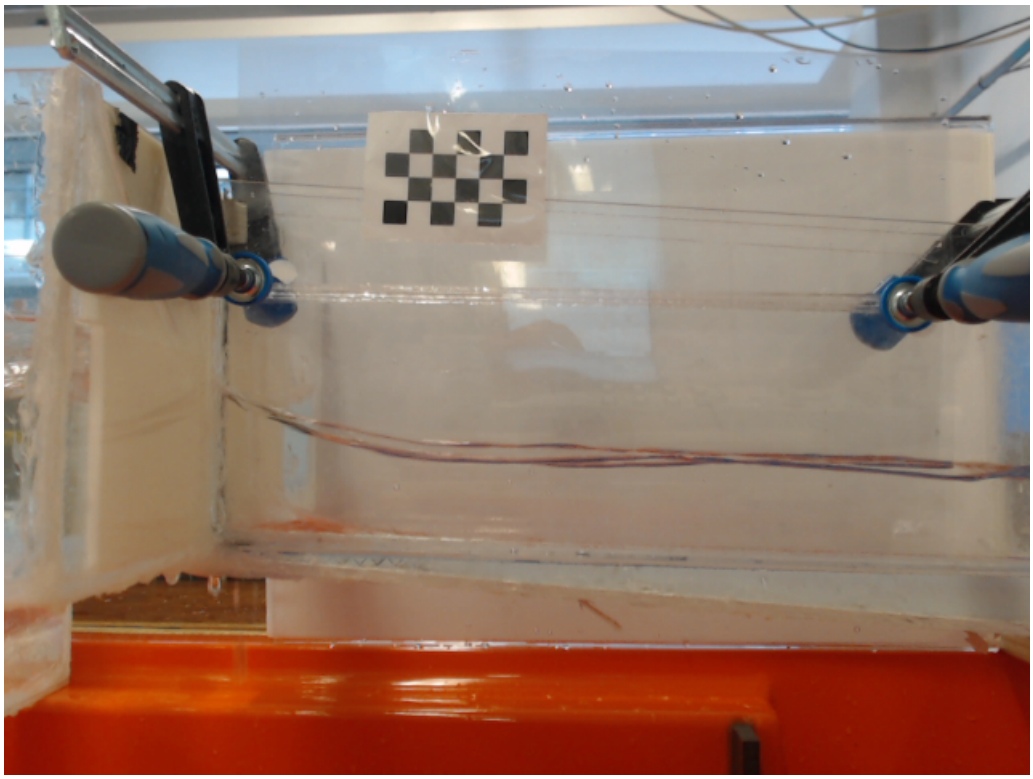

Figure 4.5: Dynamic response of mid-flow walls;

4.2 Second Phase: Data for Consolidated Model

In the second phase of experimentation, efforts were focussed on gathering a reasonably large amount of data to form the basis for experimental inference of a dimensionless model

for the flow. Some data were already available from previous work completed by Pay [5] and so this was incorporated into the final data set, although processing of the experimental images was altered to obtain a more accurate estimate of transition length. In addition to the parameters considered by Pay, only one other parameter was added: number of walls in flow. As described in Section 4.1.4, a number of parallel-to-flow walls could be added to the channel body to effectively increase the friction experienced by the flow. Despite the difficulties described in Section 4.1.4, it was still possible to extract an estimated transition length from a number of experiments using the method described herein.

4.2.1 Post-processing: Depth and Transition Length

Depth

Depth at transition and channel entry are calculated simply using the ratio of depth to rig height in pixel space in conjunction with known dimensions of the rig. This is completed using a MATLAB script to specify the relevant locations in pixel space one experiment at a time.

Transition Length

The methods described in this Section are based on a body of programming work completed by Pay [5]. While some alterations have been made to the transition length calculation algorithm, the base code is taken from Pay. The key steps of the transition length calculation are given below:

1. An image of the experiment of interest is read into MATLAB;
2. The channel floor line is defined by two user selected points (this need only be done once for every batch of experiments where the camera has not been moved relative to the rig);
3. A Canny edge filter is run over the whole image to convert it to a black and white outline image;
4. The user selects four points which encompass the majority of the free surface profile and as little extra noise as possible;
5. The image domain profile is transformed onto a dimensioned Cartesian coordinate system using a checker-board calibration. The calibration involves scaling and rotation;
6. The Cartesian domain profile then estimated as an exponential curve. The transition length is taken as the length coordinate at which the exponential fit intersects 105% of the asymptotic height. An example of a fitted exponential curve is shown in Figure 4.6.

This process eliminates the noise caused by waves present in the near-transition part of the flow.

4.2.2 Experimental Output

After post-processing as detailed in Section 4.2.1 to find depths and measured transition length, the whole experimental output yields 8 quantities for each experiment. These are given below:

1. Width = $w \quad (\mathrm{m})$
2. Channel Slope = $\theta \quad (\mathrm{no\ units})$
3. Entry Radius = $r \quad (\mathrm{m})$
4. Flow Rate = $Q \quad (\mathrm{m^3 s^{-1}})$
5. Number of Walls = $walls \quad (\mathrm{no\ units})$
6. *Measured* Transition Length = $L_T \quad (\mathrm{m})$
7. Entry Depth = $h_0 \quad (\mathrm{m})$
8. Transition Depth = $h_\infty \quad (\mathrm{m})$

These quantities form the basis of any model derived from the experiment. They may also be useful for deriving quantities useful for the analytical model (i.e. transition depth can be used to infer a friction coefficient). For the purposes of this project, these quantities are most useful when combined in the form of dimensionless parameters. This is discussed further in Section 4.3. The full table of raw results is given in Appendix B.

4.3 Data Processing

The main goal of the experimental phase of this project is to extract a dimensionless model for the flow from known input parameters. More specifically, it is useful to be able to predict the transition length from a range of input parameters, for example those collected for each experiment and listed in Section 4.2.2. This prediction takes the form of a statistical model, where the response (y_i) is approximated by a function of predictors ($x_{i,j}$). The function of predictors is denoted $\hat{y}_i$, and is also known as the estimator.

For any model, the number of permutations of possible functions is large, including but not limited to combinations of exponentials, sums, products, logs, hyperbolics functions, trigonometric function and infinite diminishing series. This report does not aim to exhaust all these possibilities since:

1. The number of permutations is infinite;

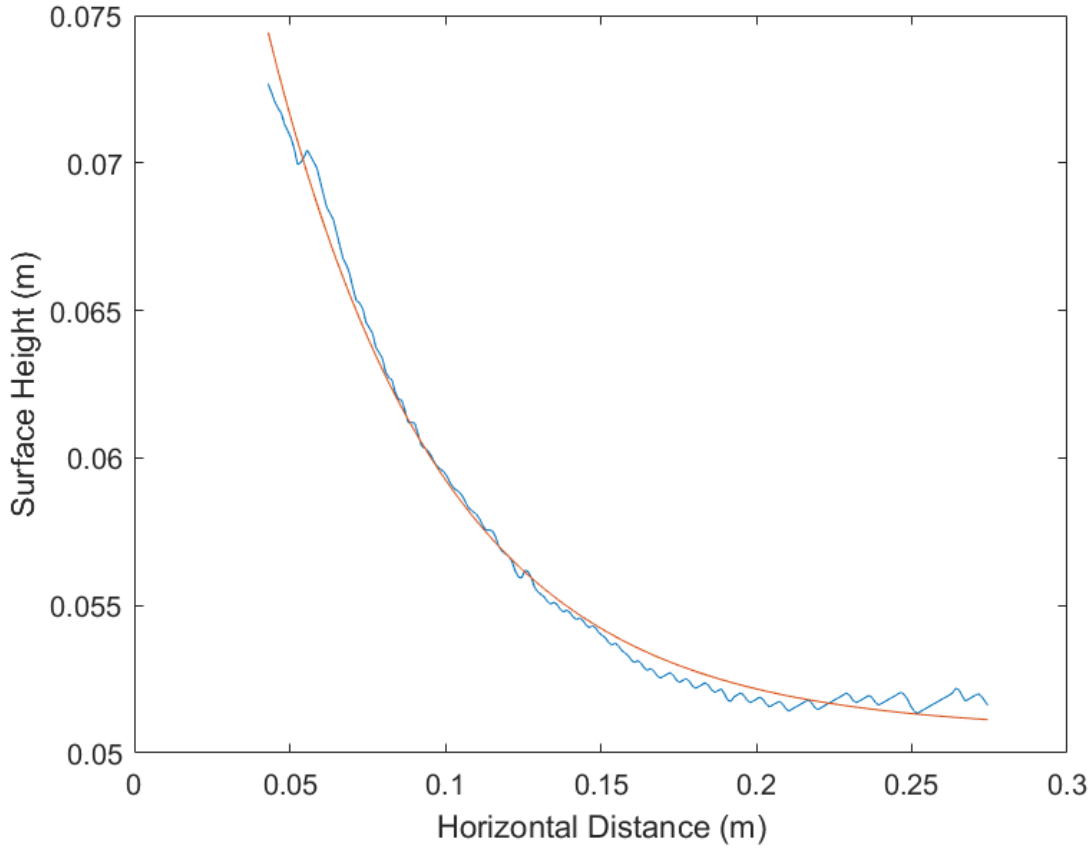

Figure 4.6: Sample exponential fit (15mm width, 10mm radius, $3.5°$ slope, 1Ls^{-1} flow rate) [note stretched axes];

2. Exhausting the infinite set of functions which could describe this model would *over-fit* the model and so model experimental noise, which is worse than useless in a predictive setting.

For these reasons, a model of the form given in Equation 4.1 is considered sensible. Other parties may wish to derive a model based on a different mathematical formulation, and can do so using the raw data given in Appendix B.

$$\underbrace{\hat{y}_i}_{Estimator} = \underbrace{-2^{n_0}}_{InterceptAdjustor} + \underbrace{2^{n_1}}_{GradientAdjustor} \left(\prod_{j=2}^{N} x_{i,j}^{n_j} \right) \tag{4.1}$$

For each experiment (label i), the transition length may be *modelled* by $\hat{y}_i$ which is a function of recorded input parameters $x_{i,j}$ with free parameters n_j.

4.3.1 Stochastic Learning

Given the functional form of the estimator given in Equation 4.1, it is now required to optimise the universally applicable free parameters, n_j. For a data set which is differentiable, this may usually be achieved by a simple gradient descent algorithm. Given that this data set is discrete and therefore not continuously differentiable, the optimisation is achieved using a custom stochastic gradient descent algorithm. The main steps of this algorithm are detailed below. The full algorithm is given in appendix C.

1. Load experimental data (or a subset of data);
2. Calculate dimensionless parameters from data;
3. Define array of responses (here a dimensionless form of transition length $= \hat{y}_i$);
4. Define array of predictors $= x_{i,j}$;
5. Initialise free parameters $= n_j$;
6. Define initial stochastic increment;
7. Define rate of increment dissipation;
8. Calculate array of estimates $= \hat{y}_i$;
9. Calculate total error $= \Sigma|\hat{y}_i - y_i|$;
10. For each free parameter:

    Increase by an amount randomly drawn from a normalised Gaussian distribution multiplied by the stochastic increment;

    Calculate new array of estimates $= \hat{y}_i^*$;

    Calculate new total error $= \sigma|\hat{y}_i^* - y_i|$;

    If total error has reduced, continue. Else, decrease free parameter by twice the

stochastic step (from item 10) and continue;

11. Diminish stochastic increment by an amount according to step 7;
12. Return to step 8 and iterate to convergence.

This algorithm optimises the set of free parameters given a defined data set, predictors and response variable. The output is also dependent on the initial values used for free parameters as the solution is simply a local optimisation. This corresponds topologically to a local minimum in N-dimensional space, which occurs less frequently than in lower dimensional space since more differentials need to equal zero to converge. Figure 4.7 shows how the 'Total Error' and the 'Response' change as the number of iterations increases.

The left hand chart plots the arbitrarily sized total error which, as expected, exhibits the following desirable features:

1. The 100 iteration rolling average of 'Total Error' decreases;
2. The minimum 'Total Error' generally decreases;
3. The noise in the error dissipates as the stochastic increment exponentially decays with iterations.
4. The 'Total Error' looks to be converging on a locally optimal model regardless of the noise dissipation (demonstrated by the relatively flat line of minima in the series);
5. Comparing the figures for one million and ten million iterations shows that one million iterations is sufficient to converge on the locally optimal solution. This discovery could save analysis time in future projects.

The right hand chart shows how the data begin to collapse onto a single line as the model becomes more accurate. This is also demonstrated by the increasing value of R^2.

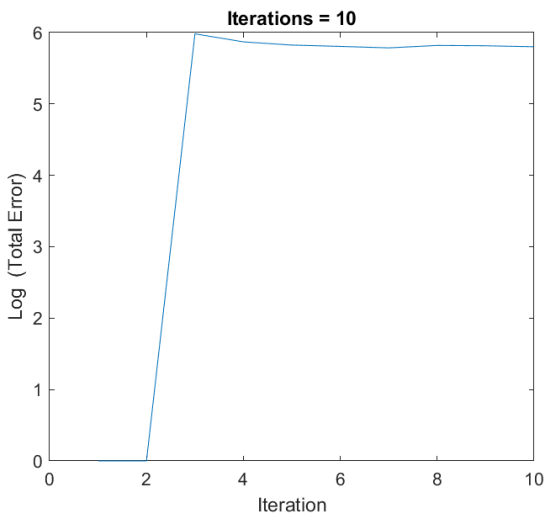

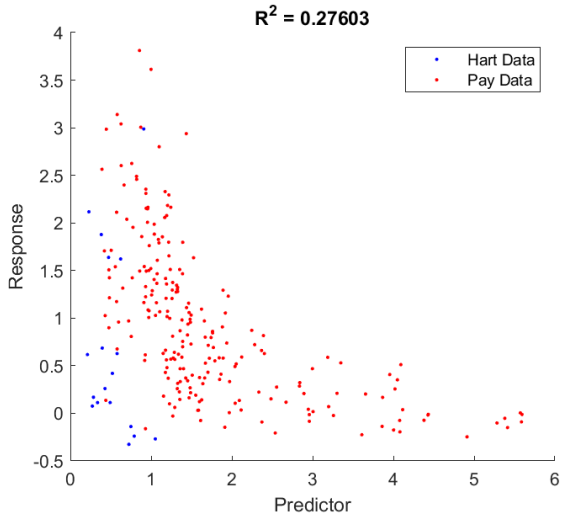

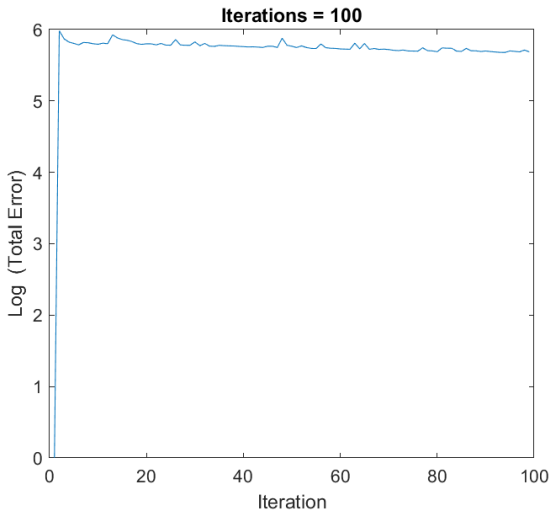
Iterations = 100
Log (Total Error)
Iteration

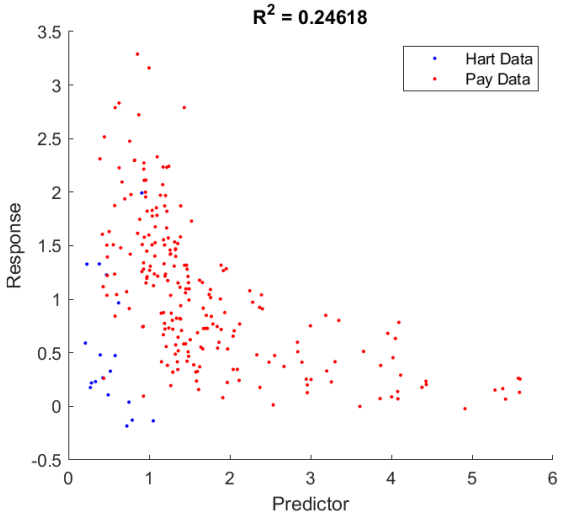
R2 = 0.24618
Hart Data
Pay Data
Response
Predictor

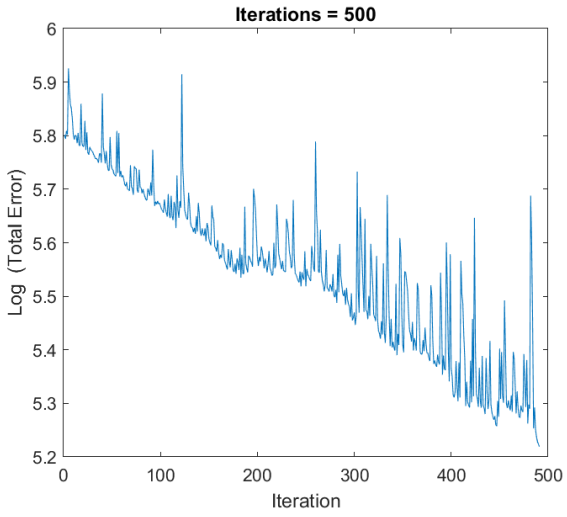
Iterations = 500
Log (Total Error)
Iteration

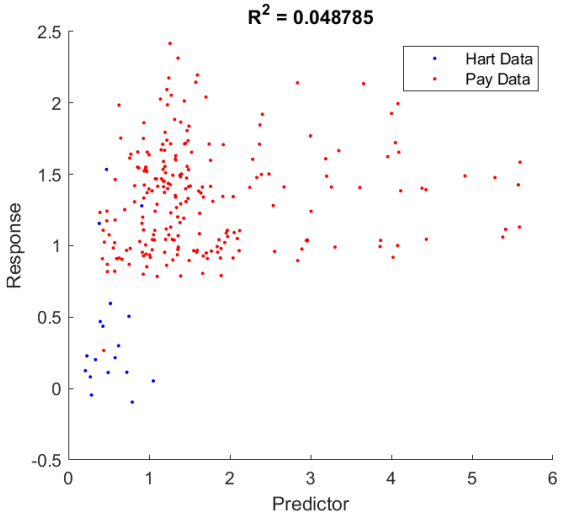
R2 = 0.048785
Hart Data
Pay Data
Response
Predictor

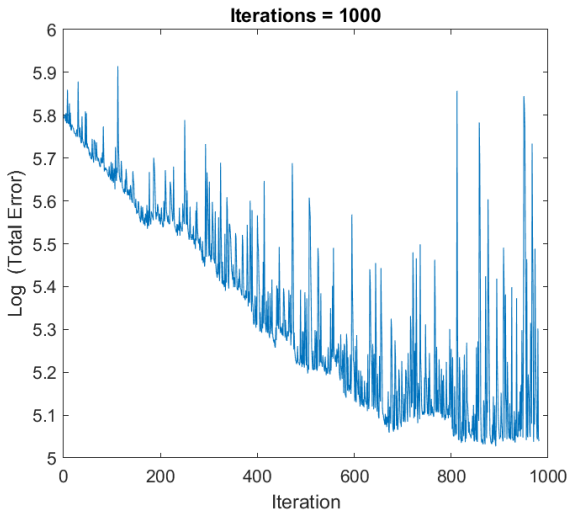
Iterations = 1000
Log (Total Error)
Iteration

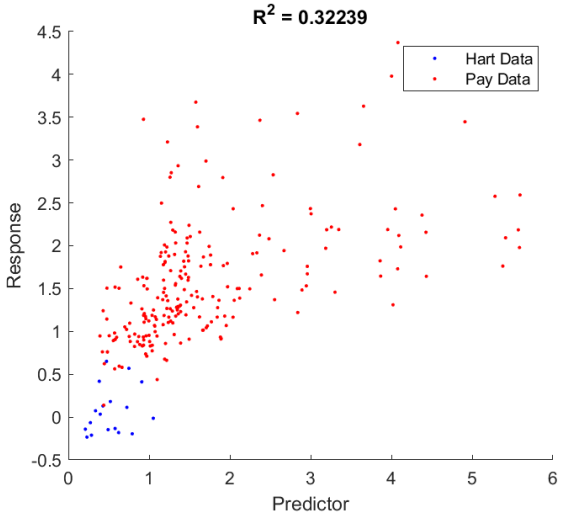
R2 = 0.32239
Hart Data
Pay Data
Response
Predictor

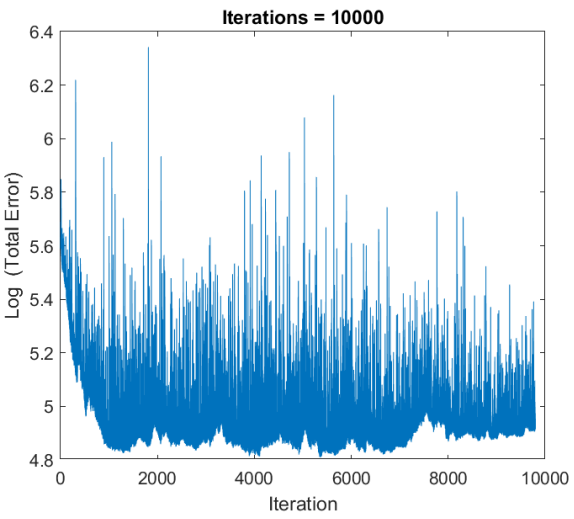
Iterations = 10000
Log (Total Error)
Iteration

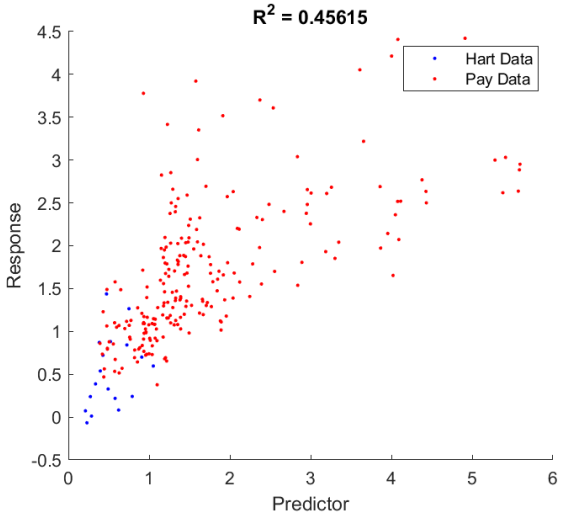
R2 = 0.45615
Hart Data
Pay Data
Response
Predictor

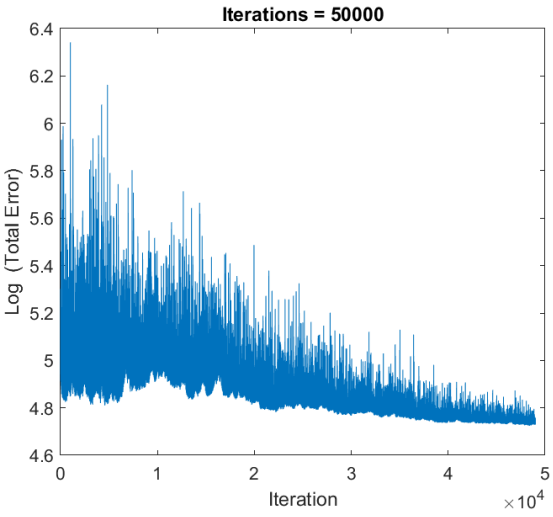
Iterations = 50000
Log (Total Error)
Iteration
×10^4

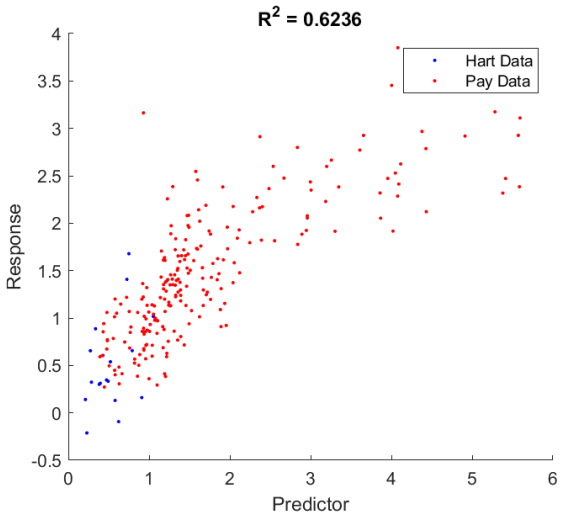
R2 = 0.6236
Hart Data
Pay Data
Response
Predictor

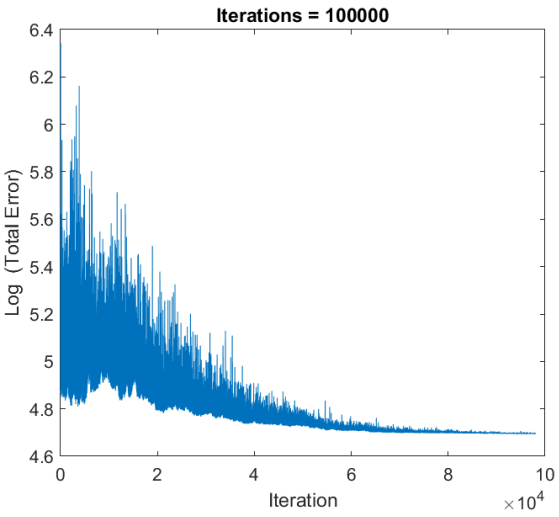
Iterations = 100000
Log (Total Error)
Iteration
×10^4

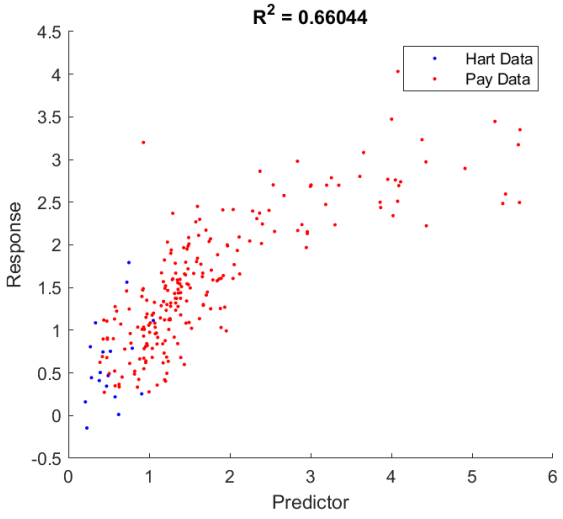
R2 = 0.66044
Hart Data
Pay Data
Response
Predictor

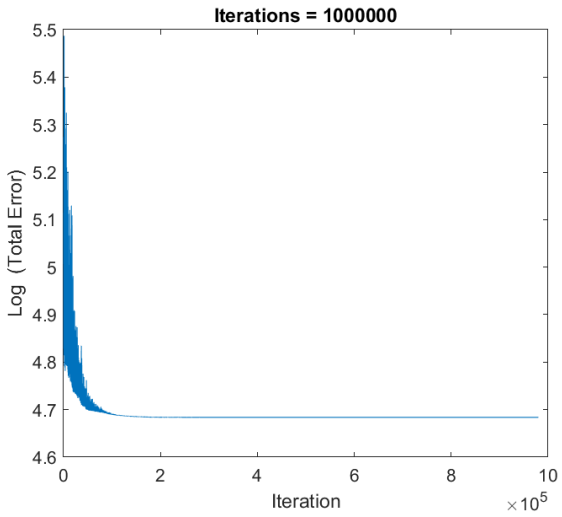

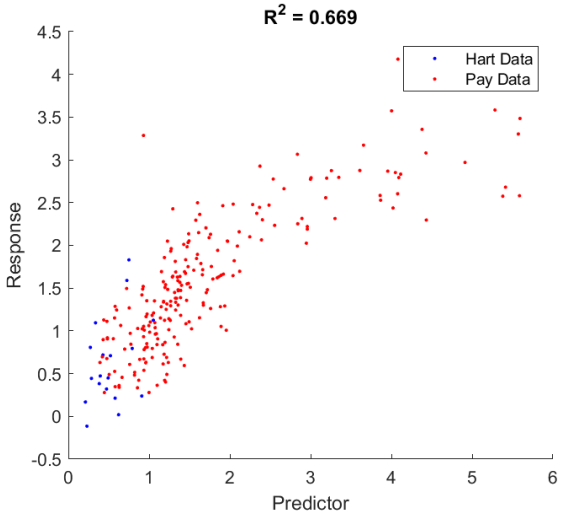

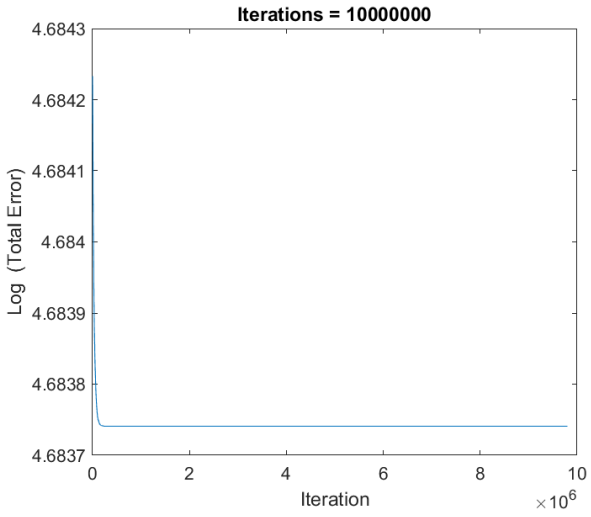

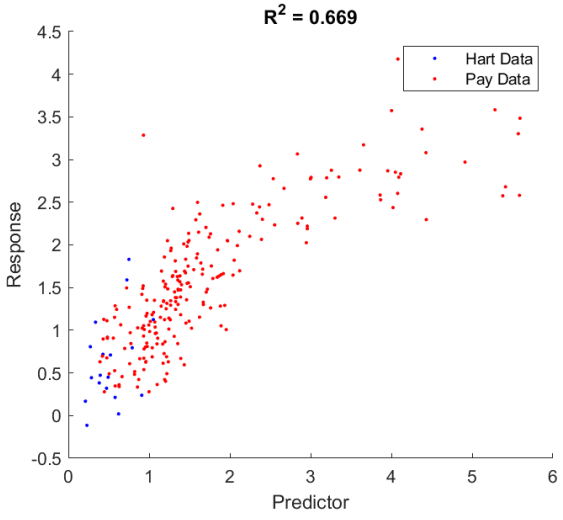

Figure 4.7: Learning progress at various stages;

Final Model

The model presented below is the best yet found for all the data collected according to the R^2 measure. This model incorporates all the data from the 242 experiments completed by the author and Pay [5]. Equation 4.1 is repeated below for context.

$$\underbrace{\hat{y}_i}_{Estimator} = \underbrace{-2^{n_0}}_{InterceptAdjustor} + \underbrace{2^{n_1}}_{GradientAdjustor} \left(\prod_{j=2}^{N} x_{i,j}^{n_j} \right) \tag{4.1}$$

The response variable used is as follows:

$$y_i = \frac{L_{t,measured,i}}{w_i} \tag{4.2}$$

The predictors used are as follows:

$$x_{i,j=[0:N]} = \vec{x}_i = \left\{ \begin{matrix} x_0 \\ x_1 \\ x_2 \\ x_3 \\ x_4 \\ x_5 \\ x_6 \\ x_7 \\ x_8 \end{matrix} \right\} = \left\{ \begin{matrix} 2 \\ 2 \\ Re_0 \\ Fr_0 \\ w* \\ \text{slope parameter} \\ \text{wall parameter} \\ \text{radius parameter} \\ \text{surface drop parameter} \end{matrix} \right\} = \left\{ \begin{matrix} 2 \\ 2 \\ \frac{\rho u_0 h_0}{\mu} \\ \frac{u_0^3 w}{gQ} \\ 1 + \frac{w}{2h_0} \\ \sin\theta \\ n_{walls} + 1 \\ \frac{r+w}{h_0} \\ \frac{h_0}{h_\infty} \end{matrix} \right\} \tag{4.3}$$

The predictors chosen for this model have been chosen carefully in order that many alternative dimensionless quantities may be formed by combining powers of the predictors. Some predictors, for example Fr_0 & $w*$, have been chosen to align with dimensionless parameters that appear in the governing equation derived in Section 3. Notably the Reynolds number does not appear explicitly in the analysis of the governing equation, however the friction factor will be a function of Reynolds.

The optimised free parameters after 10 million iterations are as follows:

$$n_{j=[0:N]} = \vec{n} = \begin{Bmatrix} n_0 \\ n_1 \\ n_2 \\ n_3 \\ n_4 \\ n_5 \\ n_6 \\ n_7 \\ n_8 \end{Bmatrix} = \begin{Bmatrix} -2.1297 \\ -2.8327 \\ 0.2639 \\ -0.5516 \\ -3.6967 \\ 0.4436 \\ -0.4801 \\ 0.4376 \\ -1.6773 \end{Bmatrix} \tag{4.4}$$

The value of R^2 for this model is as follows:

$$R^2 = 0.669 \tag{4.5}$$

5. Model Consolidation

This project is primarily focussed on the transition length in an open channel flow. Throughout the course of the project, three series of transition length have been calculated by various means. These are:

1. $L_{t,measured}$ - Measured transition length from experiments (Section 4.2);
2. $L_{t,theoretical}$ - Theoretical transition length from analytical model (Section 3.3);
3. $L_{t,modelled}$ - Modelled transition length using experimental predictors (Section 4.3.1).

Ideally, the model, experiment and theory should all match, giving the same prediction of transition length for all investigated scenarios. Figure 5.1 shows how the three versions of transition length vary by experiment. There is not good agreement between the derived theory and the experiments. Figure 4.7 shows however that a reasonable fit is obtained between the statistical model and the experiment, although the model has been tuned specifically in order to satisfy this requirement. There are a number of reasons why the theoretical model may not accurately predict what is observed in practice:

1. The derived analytical equation from Section 3.3 uses a hydrostatic model for pressure, which as shown in Section 3.1.1 relies on low Froude number, shallow slope, low curvature and a low coefficient of friction. As such these assumptions create error in the transition length predicted analytically. Section 5.1 discusses how these assumptions are not valid for the experimental data gathered.
2. The experimental procedure is prone to error in data capture. The true steady surface profile of the water is estimated as described in Section 4.2. This estimate is prone to a high degree of error due to the waves and 3-dimensional effects that are not accounted for in the idealised model.
3. Due to the unexpected halting of experimental work after March 2020 due to the COVID-19 epidemic, less data were collected for variations of identified key variables than originally intended. This has limited the insight derived from the statistical model.

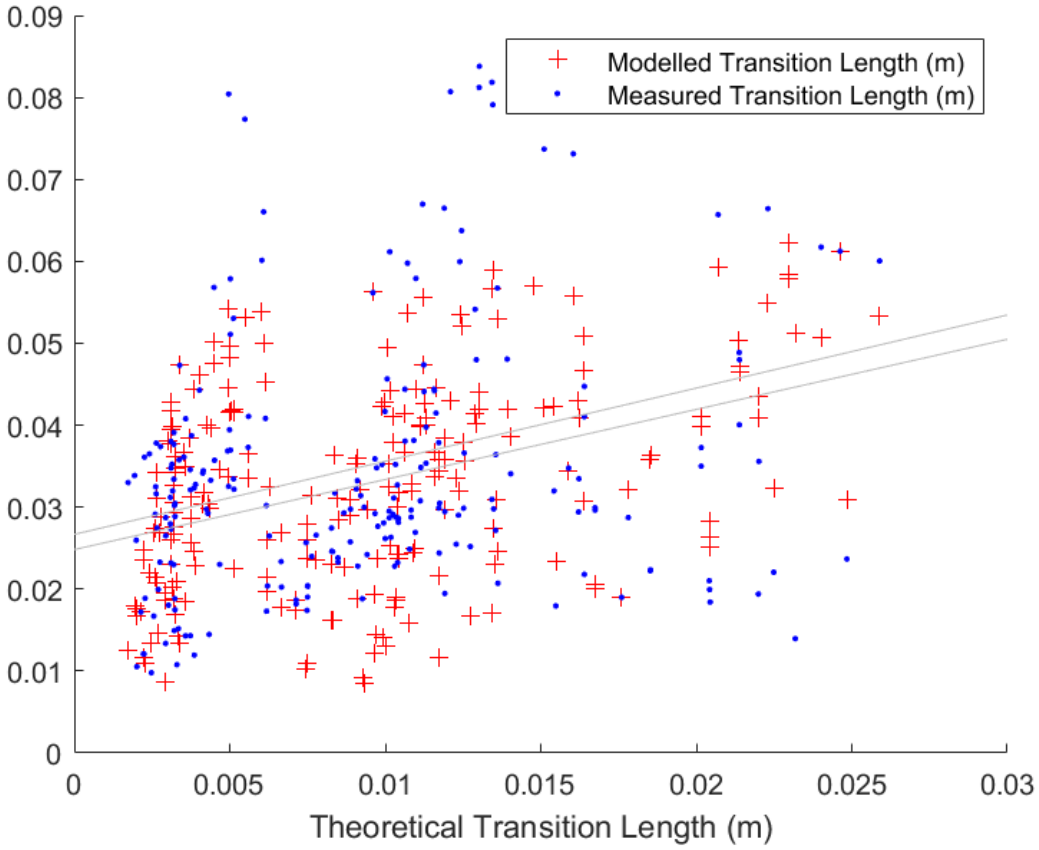

Figure 5.1: Three transition lengths compared across experiments;

5.1 Comparison of Experimental Data to Analytical Model

This section compares surface height data for the experiment with the following parameters:

$$w = 15\text{mm}; \quad \theta = 2^{\circ}; \quad r = 10\text{mm}; \quad Q = 1\text{Ls}^{-1} \tag{5.1}$$

Using data-derived values for h_0 and h_∞, it is possible to calculate Fr, C_f, p, q and all other relevant parameters as inputs to the analytical model.

Figure 5.2 shows the poor agreement between the analytical model and the implied/actual experimental data if the analytical model is anchored to the point $[x = 0, h = h_0]$. The values plotted for gradient, $\frac{dh}{dx}$, and curvature, $\frac{d^2h}{dx^2}$, show how assumptions given in figure 3.3 are violated close to the beginning of the flow.

Figures 5.3 and 5.4 show how the fit becomes more realistic as the implied experimental curvature and gradient approach zero, although here the flatness of the data superposed with experimental noise make it difficult to make too firm a judgement.

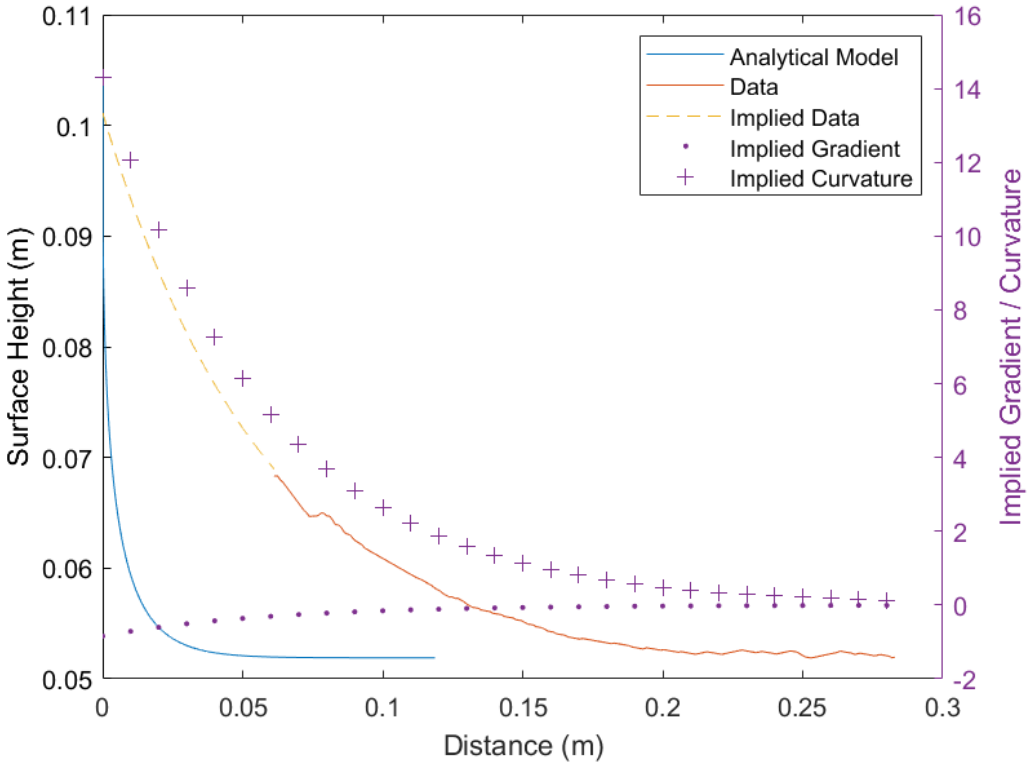

Figure 5.2: Experimental data and analytical model compared with 'start' points matched;

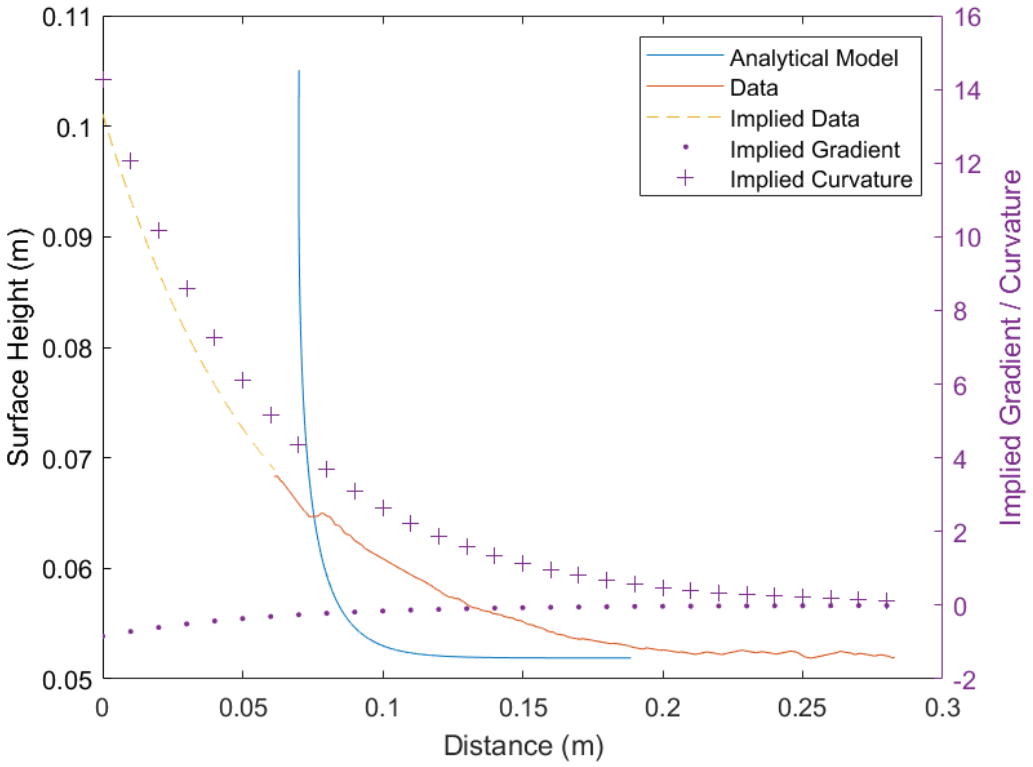

Figure 5.3: Experimental data and analytical model compared with shifted analytical start point;

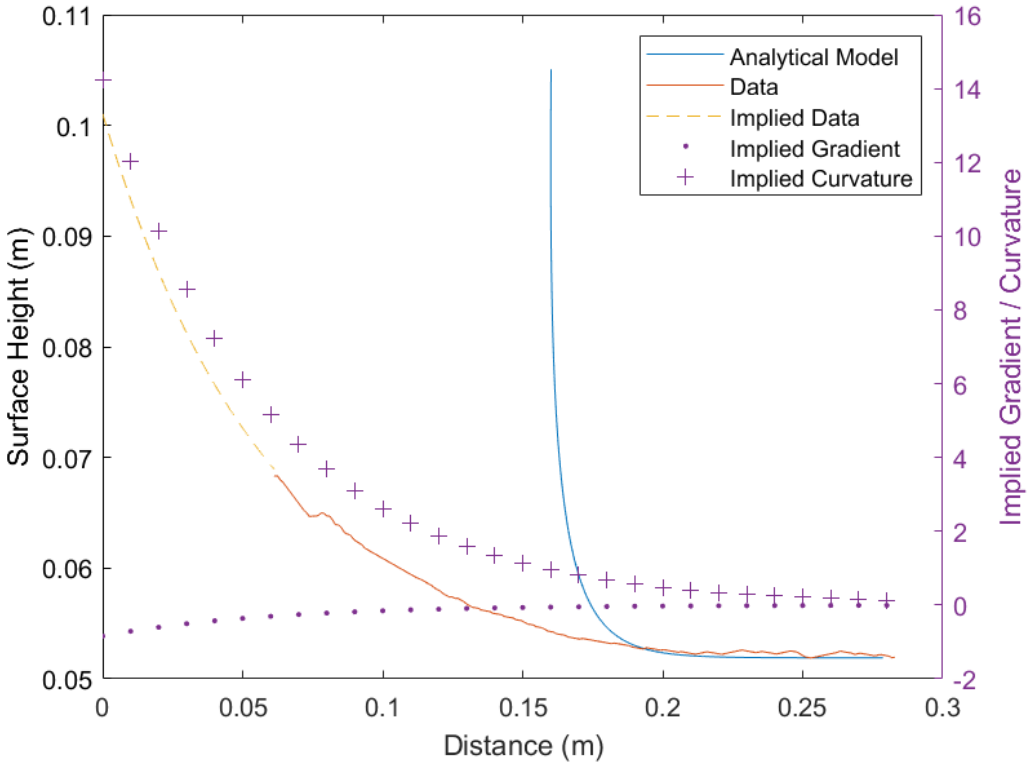

Figure 5.4: Experimental data and analytical model compared with more shifted analytical start point;

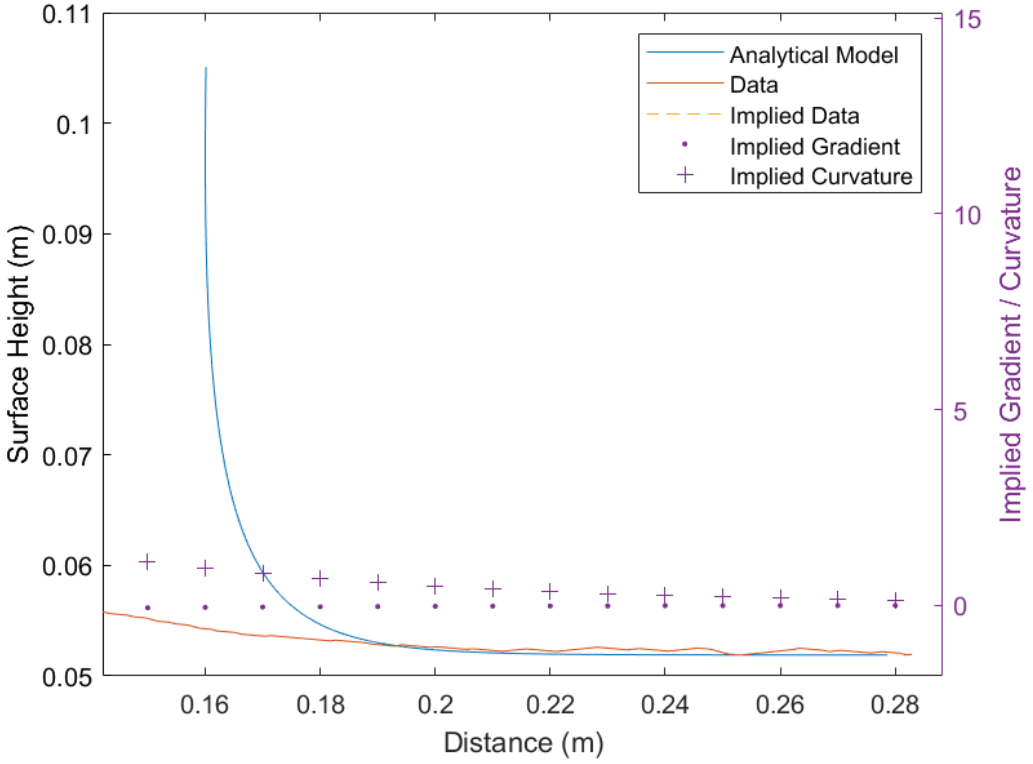

Figure 5.5: Figure 5.4 zoomed;

6. Conclusion

6.1 Outcomes

6.1.1 Analytical

Significant progress has been made in this project on the derivation of an ordinary differential equation modelling the surface height of a rapidly varying open channel flow (see Section 3). This bulk velocity model has been derived in different forms, each with different assumptions which have been clearly listed so they might be used appropriately. The most simple form, the hydrostatic model, has been fully solved to produce an explicit surface profile equation, repeated below:

$$x^{\star} = 2\sin\theta\left\{y + \frac{\left(p^3-q^3\right)}{6q^2}\left[-2\log\left(y-q\right) + \log\left(y^2+qy+q^2\right) + 2\sqrt{3}\arctan\left(\frac{2y+q}{q^2\sqrt{3}}\right)\right] + K\right\} \quad (3.43)$$

An unsolved ordinary differential equation for surface profile has also been derived, repeated below:

$$-\frac{1}{h}\left(\frac{Q}{wh}\right)^2\frac{dh}{dx} = -\frac{1}{\rho}\frac{d\overline{p}}{dx} + g\sin\theta - C_f\left(\frac{Q}{wh}\right)^2\frac{1}{2h+w} \quad (3.39)$$

where:

$$\frac{1}{\rho}\overline{p}(x) = \underbrace{\frac{h}{2}g\cos\theta}_{\text{Hydrostatic}} + \frac{1}{24}\left(\frac{Q}{wh}\right)^2\left(\underbrace{h\frac{d^2h}{dx^2}}_{\text{Curvature}} + \left(\frac{dh}{dx}\right)^2\left(\underbrace{\frac{C_f\cdot h}{2h+w}}_{Viscous} - \underbrace{1}_{Advective}\right)\right) \quad (3.21)$$

6.1.2 Experimental

A statistical model to describe the transition length using various input parameters has been derived using experimental data (see Section 4.3). This model is summarised by the following

repeated equations:

$$\underbrace{\hat{y}_i}_{Estimator} = \underbrace{-2^{n_0}}_{InterceptAdjustor} + \underbrace{2^{n_1}}_{GradientAdjustor} \left(\prod_{j=2}^{N} x_{i,j}^{n_j} \right) \tag{4.1}$$

$$y_i = \frac{L_{t,measured,i}}{w_i} \tag{4.2}$$

$$x_{i,j=[0:N]} = \vec{x}_i = \begin{Bmatrix} x_0 \\ x_1 \\ x_2 \\ x_3 \\ x_4 \\ x_5 \\ x_6 \\ x_7 \\ x_8 \end{Bmatrix} = \begin{Bmatrix} 2 \\ 2 \\ Re_0 \\ Fr_0 \\ w* \\ \text{slope parameter} \\ \text{wall parameter} \\ \text{radius parameter} \\ \text{surface drop parameter} \end{Bmatrix} = \begin{Bmatrix} 2 \\ 2 \\ \frac{\rho u_0 h_0}{\mu} \\ \frac{u_0^3 w}{gQ} \\ 1 + \frac{w}{2h_0} \\ \sin\theta \\ n_{walls} + 1 \\ \frac{r+w}{h_0} \\ \frac{h_0}{h_\infty} \end{Bmatrix} \tag{4.3}$$

$$n_{j=[0:N]} = \vec{n} = \begin{Bmatrix} n_0 \\ n_1 \\ n_2 \\ n_3 \\ n_4 \\ n_5 \\ n_6 \\ n_7 \\ n_8 \end{Bmatrix} = \begin{Bmatrix} -2.1297 \\ -2.8327 \\ 0.2639 \\ -0.5516 \\ -3.6967 \\ 0.4436 \\ -0.4801 \\ 0.4376 \\ -1.6773 \end{Bmatrix} \tag{4.4}$$

$$R^2 = 0.669 \tag{4.5}$$

While the agreement between the statistical model and the measured data is good, there is very little agreement between the analytical model and either the measured or modelled transition length.

6.2 Future Work

The project is now the third to look into this problem and the physics are still not sufficiently understood. The author expects that another final year project (FYP) or undergraduate research opportunity (UROP) would be sufficient to gain a solid understanding of this problem. A number of avenues are suggested for further work herein.

Analytical Model

Only the hydrostatic model of the flow has been fully resolved into an explicit surface profile, however a more comprehensive ordinary differential equation for the surface profile has been derived. Using numerical or analytical techniques, it should be possible to resolve this ODE into an explicit surface profile which may better predict the transition length of this flow.

Experimental Model

The current model that has been derived in this project fits the experimental data reasonably well, although unforeseen circumstances have forced less data to be gathered than planned for. Future parties investigating this flow are advised to gather a new set of data, preferably with hundreds of experiments, focussing on varying only a few parameters. This report has shown that entry radius, walls and restrictions are not likely to give particularly reliable insight and so the main variables such as flow rate, slope and width should be focussed upon. Additionally, Section 4.3 showed that 1 million iterations is sufficient to converge on a locally optimal model.

7. References

[1] J.V. Boussinesq. Essay on the theory of running waters. *Mémoires présentés par divers savants à l'Académie des sciences*, 23:1–660, 1877.

[2] V.T. Chow. *Open-channel hydraulics*, page 5. New Jersey: Blackburn Press, 2008. ISBN 9781932846188.

[3] M. Vazquez Calle. Experimental Investigation of Free Surface Profile in Open-Channel Flow. Technical report, Imperial Collge London, 2019.

[4] H. Hart. Rapidly Varying Open Channel Flow, Project Plan Report, ME4 Individual Project. Technical report, Imperial College London, 2019.

[5] D. Pay. Presentation: Transition length in open channel flows: Summary of work done. Technical report, Imperial College London, 2019.

[6] R. Fox, A. McDonald, and J. Pritchard. *Fluid Mechanics*, pages 610 – 619. New York: John Wiley and Sons, 2012. ISBN: 978-1-118-02641-0.

[7] B.A. Bakhmeteff. *Hydraulics of Open Channels*, page 31. New York: McGraw-Hill, 1932. ASIN: B000SMSLO2.

[8] J.S. Montes. Potential flow solution to 2D transition from mild to steep slope. *Journal of Hydraulic Engineering*, 120:601–621, 1994.

[9] R. Ehrenburger. Versucher uber die verteilung der drucke an wehrrucken infolge des absturzenden wassers. *Die Wasserwirtschaft*, 22(5):65–72, 1929.

[10] M. Andersen. Transition from subcritical to supercritical flow. *Journal of Hydraulic Research*, 13:227–238, 1975.

[11] G. Formica. Preliminary tests on head losses in channels due to cross-sectional changes. *L'Energia Ellectrica*, 32(7):554–568, 1955.

[12] F. Dias and J. Vanden-Broeck. Open channel flows with submerged obstructions. *Journal of Fluid Mechanics*, 206:155 – 170, 1989.

[13] O. Reynolds. On the dynamical theory of incompressible viscous fluids and the determination of the criterion. *Philosophical Transactions of the Royal Society of London A.*, 186:123–164, 1895. doi: $10.1098/\mathrm{rsta}.1895.0004$.

[14] F. White. *Fluid Mechanics*, pages 477–478. New York: McGraw-Hill, 2011. ISBN: 978-0-071-31121-2.

[15] L. Prantl. Bericht uber Untersuchungen zur ausgebildeten Turbulenz. *Zeitschrift fur angew. Math. u. Mechanik*, 5:136–139, 1925.

[16] L.F. Moody. Friction factors for pipe flow. *Transactions of the ASME*, 66:671–684, 1944.

A. Differential Equation Solution Derivation

$$\frac{\mathrm{d}}{\mathrm{d}x}\left(\frac{\mathrm{Fr}.u^2}{\cos\theta}+u^{-1}\right)=2\tan\theta-\frac{C.\mathrm{Fr}.u^3}{\cos\theta} \tag{A.1}$$

Let $y=1/u$,

$$\frac{\mathrm{d}}{\mathrm{d}x}\left(\frac{\mathrm{Fr}.y^{-2}}{\cos\theta}+y\right)=2\tan\theta-\frac{C.\mathrm{Fr}.y^{-3}}{\cos\theta} \tag{A.2}$$

Multiply by y^3 and use the chain rule,

$$y^3\frac{\mathrm{d}y}{\mathrm{d}x}\frac{\mathrm{d}}{\mathrm{d}y}\left(\frac{\mathrm{Fr}.y^{-2}}{\cos\theta}+y\right)=2y^3\tan\theta-\frac{C\mathrm{Fr}}{\cos\theta} \tag{A.3}$$

$$y^3\frac{\mathrm{d}y}{\mathrm{d}x}\left(-\frac{2\mathrm{Fr}.y^{-3}}{\cos\theta}+1\right)=2y^3\tan\theta y^3-\frac{C\mathrm{Fr}}{\cos\theta} \tag{A.4}$$

Separate variables, then substitute $p^3=2\mathrm{Fr}/\cos\theta$; $q^3=C\mathrm{Fr}/2\sin\theta$:

$$\mathrm{d}x=\frac{\left(y^3-\frac{2\mathrm{Fr}}{\cos\theta}\right)}{\left(2y^3\tan\theta-\frac{C\mathrm{Fr}}{\cos\theta}\right)}\mathrm{d}y=\frac{\left(y^3-p^3\right)}{\left(y^3-q^3\right)}\frac{\mathrm{d}y}{2\sin\theta} \tag{A.5}$$

Note for $\mathrm{d}y/\mathrm{d}x=0$, $y=q$. To integrate, substitute $z=2\sin\theta x$, $y=q\zeta$, and $p^3/q^3=(1-\eta)$

$$\mathrm{d}z=\frac{\zeta^3-(1-\eta)}{\zeta^3-1}q\mathrm{d}\zeta \tag{A.6}$$

Rearranging into partial fractions

$$\frac{\zeta^3-(1-\eta)}{\zeta^3-1}=\frac{\zeta^3}{\zeta^3-1}-\frac{(1-\eta)}{\zeta^3-1}=1+\frac{1-(1-\eta)}{\zeta^3-1}=1+\frac{\eta}{\zeta^3-1} \tag{A.7}$$

$$=1+\eta\frac{\alpha}{\zeta-1}+\eta\frac{\beta\zeta+\gamma}{\zeta^2+\zeta+1} \tag{A.8}$$

Solution for partial fractions: $\alpha=1/3,\beta=-1/3,\gamma=-2/3$:

$$\frac{\zeta^3-(1-\eta)}{\zeta-1}=1+\frac{\eta}{3\left(\zeta-1\right)}-\frac{\eta\left(\zeta+2\right)}{3\left(\zeta^2+\zeta+1\right)} \tag{A.9}$$

$$=1+\frac{\eta}{3\left(\zeta-1\right)}-\frac{\eta\left(2\zeta+1\right)}{6\left(\zeta^2+\zeta+1\right)}+\frac{\eta}{2\left(\zeta^2+\zeta+1\right)} \tag{A.10}$$

$$= 1 + \frac{\eta}{3(\zeta - 1)} - \frac{\eta(2\zeta + 1)}{6(\zeta^2 + \zeta + 1)} + \frac{\eta}{2((\zeta + 1/2)^2 + 3/4)}. \tag{A.11}$$

Integrating Equation A.7 [1], [2]:

$$z = q\zeta + \frac{\eta q}{3}\log(\zeta - 1) - \frac{\eta q}{6}\log\left(\zeta^2 + \zeta + 1\right) - \frac{\eta q\sqrt{3}}{3}\arctan\left(\frac{2\zeta + 1}{q\sqrt{3}}\right) + K. \tag{A.12}$$

Substitute $z = x/2\sin\theta$, $\zeta = y/q$, and $\eta q = q - p^3/q^2 = \left(q^3 - p^3\right)/q^2$:

$$x = 2\sin\theta\left\{y + \frac{\left(q^3 - p^3\right)}{6q^2}\left[2\log(y/q - 1) - \log\left(\frac{y^2}{q^2} + \frac{y}{q} + 1\right) - 2\sqrt{3}\arctan\left(\frac{2y+q}{q^2\sqrt{3}}\right)\right] + K\right\} \tag{A.13}$$

$$x = 2\sin\theta\left\{y + \frac{\left(p^3 - q^3\right)}{6q^2}\left[-2\log(y - q) + \log\left(y^2 + qy + q^2\right) + 2\sqrt{3}\arctan\left(\frac{2y+q}{q^2\sqrt{3}}\right)\right] + K\right\} \tag{A.14}$$

[3]

[1] $\int \frac{2\zeta+1}{\zeta^2+\zeta+1}\mathrm{d}\zeta = \int \frac{f'(\zeta)}{f(\zeta)}\mathrm{d}\zeta = \log(f(\zeta))$

[2] $\int \frac{1}{(\zeta+1/2)^2+3/4}\mathrm{d}\zeta = \frac{2\sqrt{3}}{3}\int \frac{1}{u^2+1}\mathrm{d}u$ where $u = \frac{2x}{\sqrt{3}}$

[3] $2\log A - \log B = 2\log A + 2\log q - \log q^2 - \log B = 2\log Aq - \log Bq^2$

B. Detailed Results

Table B.1: Detailed results;

Note	w (mm)	θ (deg)	r (mm)	Q (mm/s)	n_{walls}	$L_{t,measured}$	$h_{0,measured}$	$h_{\infty,measured}$
Hart40	30	3.5	10	442.7	5	0.0273	0.3068	0.1806
Hart41	30	3.5	10	819.4	5	0.0142	0.4138	0.2174
Hart44	30	3.5	10	229.7	2	0.0069	0.1545	0.0880
Hart45	30	3.5	10	338.9	5	0.0187	0.2103	0.1507
Hart46	30	3.5	10	519.7	0	0.0063	0.2398	0.1308
Hart47	30	3.5	10	596.7	2	0.0174	0.2743	0.1822
Hart48	20	3.5	10	610	0	0.0158	0.2893	0.1982
Hart49	30	3.5	10	631	5	0.0115	0.3648	0.2222
Hart50	30	3.5	10	694.9	0	0.0086	0.2775	0.1826
Hart51	30	3.5	10	795.7	5	0.0118	0.3652	0.2706
Hart52	20	3.5	10	884.6	0	0.0210	0.3808	0.2381
Hart53	30	3.5	10	963.2	2	0.0148	0.3462	0.2488
Hart54	30	3.5	10	1016.7	0	0.0082	0.3660	0.2308
Hart55	20	3.5	10	1143.8	0	0.0150	0.5336	0.2905
Hart56	30	3.5	10	1168.1	0	0.0101	0.4224	0.2591
Hart57	30	3.5	10	1168.1	5	0.0156	0.4635	0.3318
Hart58	30	3.5	10	1193.5	2	0.0129	0.4407	0.2857
Hart59	20	3.5	10	1220	0	0.0145	0.4758	0.2952
Hart60	30	3.5	10	1220	0	0.0132	0.4402	0.2615
Daryl1	15	3.5	0	500	0	0.0184	0.4747	0.1946
Daryl2	15	3.5	0	600	0	0.0237	0.5354	0.2148
Daryl3	15	3.5	0	700	0	0.0356	0.5859	0.2550
Daryl4	15	3.5	0	800	0	0.0140	0.6313	0.2819
Daryl5	15	3.5	0	900	0	0.0600	0.6919	0.3020
Daryl6	15	3.5	0	1000	0	0.0612	0.7576	0.3356
Daryl7	15	3.5	6	400	0	0.0179	0.4040	0.1745
Daryl8	15	3.5	6	500	0	0.0199	0.4596	0.1946
Daryl9	15	3.5	6	600	0	0.0221	0.5101	0.2215
Daryl10	15	3.5	6	700	0	0.0194	0.5657	0.2550
Daryl11	15	3.5	6	800	0	0.0489	0.6162	0.2886
Daryl12	15	3.5	6	900	0	0.0657	0.6717	0.3221
Daryl13	15	3.5	6	1000	0	0.0792	0.7222	0.3423
Daryl14	15	3.5	8	400	0	0.0207	0.4091	0.1812
Daryl15	15	3.5	8	500	0	0.0218	0.4596	0.2081

Daryl16	15	3.5	8	600	0	0.0223	0.5152	0.2349
Daryl17	15	3.5	8	700	0	0.0373	0.5758	0.2617
Daryl18	15	3.5	8	800	0	0.0480	0.6263	0.2886
Daryl19	15	3.5	8	900	0	0.0664	0.6667	0.3154
Daryl20	15	3.5	8	1000	0	0.0839	0.7374	0.3423
Daryl21	15	3.5	10	400	0	0.0190	0.4091	0.1678
Daryl22	15	3.5	10	500	0	0.0210	0.4545	0.1946
Daryl23	15	3.5	10	600	0	0.0222	0.5101	0.2349
Daryl24	15	3.5	10	700	0	0.0350	0.5758	0.2617
Daryl25	15	3.5	10	800	0	0.0401	0.6212	0.2886
Daryl26	15	3.5	10	900	0	0.0617	0.6616	0.3087
Daryl27	15	3.5	10	1000	0	0.0836	0.7222	0.3423
Daryl28	15	2	0	400	0	0.0173	0.4213	0.1929
Daryl29	15	2	0	500	0	0.0190	0.4619	0.2214
Daryl30	15	2	0	600	0	0.0242	0.5228	0.2429
Daryl31	15	2	0	700	0	0.0287	0.5736	0.2714
Daryl32	15	2	0	800	0	0.0381	0.6193	0.3000
Daryl33	15	2	0	900	0	0.0541	0.6701	0.3143
Daryl34	15	2	0	1000	0	0.0737	0.7157	0.3286
Daryl35	15	2	6	400	0	0.0182	0.3959	0.1857
Daryl36	15	2	6	500	0	0.0203	0.4467	0.2214
Daryl37	15	2	6	600	0	0.0238	0.4975	0.2500
Daryl38	15	2	6	700	0	0.0295	0.5584	0.2714
Daryl39	15	2	6	800	0	0.0444	0.5939	0.2929
Daryl40	15	2	6	900	0	0.0579	0.6447	0.3286
Daryl41	15	2	6	1000	0	0.0812	0.6954	0.3429
Daryl42	15	2	8	400	0	0.0204	0.4010	0.1929
Daryl43	15	2	8	500	0	0.0202	0.4518	0.2286
Daryl44	15	2	8	600	0	0.0240	0.5076	0.2571
Daryl45	15	2	8	700	0	0.0317	0.5584	0.2857
Daryl46	15	2	8	800	0	0.0444	0.6041	0.3000
Daryl47	15	2	8	900	0	0.0612	0.6548	0.3357
Daryl48	15	2	8	1000	0	0.0838	0.7005	0.3429
Daryl49	15	2	10	400	0	0.0187	0.3959	0.1857
Daryl50	15	2	10	500	0	0.0204	0.4518	0.2214
Daryl51	15	2	10	600	0	0.0233	0.5025	0.2500
Daryl52	15	2	10	700	0	0.0314	0.5635	0.2786
Daryl53	15	2	10	800	0	0.0442	0.5990	0.2929
Daryl54	15	2	10	900	0	0.0665	0.6497	0.3214
Daryl55	15	2	10	1000	0	0.0807	0.7005	0.3500
Daryl56	20	3.5	0	400	0	0.0252	0.3819	0.1438
Daryl57	20	3.5	0	500	0	0.0272	0.4372	0.1712
Daryl58	20	3.5	0	600	0	0.0255	0.4874	0.2055
Daryl59	20	3.5	0	700	0	0.0341	0.5327	0.2260
Daryl60	20	3.5	0	800	0	0.0320	0.5879	0.2466
Daryl61	20	3.5	0	900	0	0.0567	0.6432	0.2808
Daryl62	20	3.5	0	1000	0	0.0731	0.6784	0.2945

Daryl63	20	3.5	6	400	0	0.0266	0.3719	0.1644
Daryl64	20	3.5	6	500	0	0.0297	0.4221	0.1918
Daryl65	20	3.5	6	600	0	0.0290	0.4724	0.2055
Daryl66	20	3.5	6	700	0	0.0299	0.5327	0.2329
Daryl67	20	3.5	6	800	0	0.0481	0.5829	0.2534
Daryl68	20	3.5	6	900	0	0.0600	0.6281	0.2877
Daryl69	20	3.5	6	1000	0	0.0810	0.6583	0.3014
Daryl70	20	3.5	8	400	0	0.0228	0.3869	0.1575
Daryl71	20	3.5	8	500	0	0.0263	0.4372	0.1849
Daryl72	20	3.5	8	600	0	0.0296	0.4824	0.2123
Daryl73	20	3.5	8	700	0	0.0349	0.5327	0.2397
Daryl74	20	3.5	8	800	0	0.0474	0.5829	0.2671
Daryl75	20	3.5	8	900	0	0.0670	0.6281	0.2945
Daryl76	20	3.5	8	1000	0	0.0791	0.6583	0.3082
Daryl77	20	3.5	10	400	0	0.0249	0.3869	0.1507
Daryl78	20	3.5	10	500	0	0.0244	0.4422	0.1781
Daryl79	20	3.5	10	600	0	0.0288	0.4824	0.2123
Daryl80	20	3.5	10	700	0	0.0352	0.5327	0.2466
Daryl81	20	3.5	10	800	0	0.0456	0.5829	0.2740
Daryl82	20	3.5	10	900	0	0.0637	0.6181	0.2877
Daryl83	20	3.5	10	1000	0	0.0818	0.6633	0.3082
Daryl84	20	2	0	400	0	0.0352	0.3788	0.1773
Daryl85	20	2	0	500	0	0.0334	0.4141	0.1915
Daryl86	20	2	0	600	0	0.0302	0.4646	0.2128
Daryl87	20	2	0	700	0	0.0265	0.5101	0.2411
Daryl88	20	2	0	800	0	0.0325	0.5606	0.2837
Daryl89	20	2	0	900	0	0.0408	0.6061	0.2979
Daryl90	20	2	0	1000	0	0.0601	0.6414	0.3262
Daryl91	20	2	6	400	0	0.0325	0.3687	0.1844
Daryl92	20	2	6	500	0	0.0387	0.4091	0.2057
Daryl93	20	2	6	600	0	0.0408	0.4545	0.2411
Daryl94	20	2	6	700	0	0.0373	0.4949	0.2482
Daryl95	20	2	6	800	0	0.0394	0.5505	0.2837
Daryl96	20	2	6	900	0	0.0579	0.5859	0.3121
Daryl97	20	2	6	1000	0	0.0773	0.6313	0.3333
Daryl98	20	2	8	400	0	0.0391	0.3636	0.1773
Daryl99	20	2	8	500	0	0.0334	0.4091	0.2128
Daryl100	20	2	8	600	0	0.0344	0.4495	0.2340
Daryl101	20	2	8	700	0	0.0333	0.4848	0.2624
Daryl102	20	2	8	800	0	0.0370	0.5404	0.2837
Daryl103	20	2	8	900	0	0.0511	0.5859	0.3121
Daryl104	20	2	8	1000	0	0.0660	0.6212	0.3262
Daryl105	20	2	10	400	0	0.0378	0.3636	0.1844
Daryl106	20	2	10	500	0	0.0376	0.4091	0.2128
Daryl107	20	2	10	600	0	0.0342	0.4545	0.2340
Daryl108	20	2	10	700	0	0.0369	0.5000	0.2553
Daryl109	20	2	10	800	0	0.0411	0.5505	0.2766

Daryl110	20	2	10	900	0	0.0568	0.5859	0.3191
Daryl111	20	2	10	1000	0	0.0804	0.6263	0.3404
Daryl112	25	3.5	0	400	0	0.0348	0.3266	0.1284
Daryl113	25	3.5	0	500	0	0.0277	0.3568	0.1554
Daryl114	25	3.5	0	600	0	0.0299	0.3970	0.1554
Daryl115	25	3.5	0	700	0	0.0295	0.4372	0.1959
Daryl116	25	3.5	0	800	0	0.0287	0.4724	0.1959
Daryl117	25	3.5	0	900	0	0.0294	0.5025	0.2230
Daryl118	25	3.5	0	1000	0	0.0410	0.5327	0.2432
Daryl119	25	3.5	6	400	0	0.0305	0.3166	0.1216
Daryl120	25	3.5	6	500	0	0.0309	0.3467	0.1419
Daryl121	25	3.5	6	600	0	0.0296	0.3819	0.1554
Daryl122	25	3.5	6	700	0	0.0364	0.4271	0.1892
Daryl123	25	3.5	6	800	0	0.0348	0.4573	0.2027
Daryl124	25	3.5	6	900	0	0.0335	0.4925	0.2230
Daryl125	25	3.5	6	1000	0	0.0447	0.5327	0.2432
Daryl126	25	3.5	8	400	0	0.0359	0.3367	0.1284
Daryl127	25	3.5	8	500	0	0.0292	0.3769	0.1554
Daryl128	25	3.5	8	600	0	0.0381	0.4171	0.1757
Daryl129	25	3.5	8	700	0	0.0298	0.4523	0.1892
Daryl130	25	3.5	8	800	0	0.0308	0.4874	0.2230
Daryl131	25	3.5	8	900	0	0.0480	0.5427	0.2365
Daryl132	25	3.5	8	1000	0	0.0598	0.5779	0.2703
Daryl133	25	3.5	10	400	0	0.0234	0.3216	0.1419
Daryl134	25	3.5	10	500	0	0.0274	0.3618	0.1622
Daryl135	25	3.5	10	600	0	0.0269	0.4070	0.1757
Daryl136	25	3.5	10	700	0	0.0332	0.4523	0.2095
Daryl137	25	3.5	10	800	0	0.0366	0.4874	0.2162
Daryl138	25	3.5	10	900	0	0.0415	0.5276	0.2432
Daryl139	25	3.5	10	1000	0	0.0562	0.5779	0.2770
Daryl140	25	2	0	400	0	0.0339	0.3367	0.1620
Daryl141	25	2	0	500	0	0.0108	0.3668	0.1761
Daryl142	25	2	0	600	0	0.0119	0.4171	0.1972
Daryl143	25	2	0	700	0	0.0145	0.4523	0.2183
Daryl144	25	2	0	800	0	0.0230	0.4925	0.2394
Daryl145	25	2	0	900	0	0.0298	0.5528	0.2676
Daryl146	25	2	0	1000	0	0.0357	0.5729	0.2887
Daryl147	25	2	6	400	0	0.0105	0.3216	0.1620
Daryl148	25	2	6	500	0	0.0121	0.3618	0.1901
Daryl149	25	2	6	600	0	0.0374	0.4070	0.2113
Daryl150	25	2	6	700	0	0.0188	0.4422	0.2324
Daryl151	25	2	6	800	0	0.0232	0.4774	0.2606
Daryl152	25	2	6	900	0	0.0323	0.5176	0.2746
Daryl153	25	2	6	1000	0	0.0530	0.5628	0.2817
Daryl154	25	2	8	400	0	0.0260	0.3266	0.1620
Daryl155	25	2	8	500	0	0.0121	0.3668	0.1901
Daryl156	25	2	8	600	0	0.0328	0.4070	0.1972

Daryl157	25	2	8	700	0	0.0149	0.4472	0.2324
Daryl158	25	2	8	800	0	0.0348	0.4774	0.2606
Daryl159	25	2	8	900	0	0.0473	0.5126	0.2817
Daryl160	25	2	8	1000	0	0.0322	0.5578	0.2817
Daryl161	25	2	10	400	0	0.0098	0.3367	0.1549
Daryl162	25	2	10	500	0	0.0175	0.3819	0.1761
Daryl163	25	2	10	600	0	0.0233	0.4121	0.2113
Daryl164	25	2	10	700	0	0.0143	0.4523	0.2254
Daryl165	25	2	10	800	0	0.0180	0.4975	0.2606
Daryl166	25	2	10	900	0	0.0346	0.5477	0.2746
Daryl167	25	2	10	1000	0	0.0443	0.5628	0.2958
Daryl168	30	3.5	0	400	0	0.0188	0.3015	0.1111
Daryl169	30	3.5	0	500	0	0.0281	0.3417	0.1319
Daryl170	30	3.5	0	600	0	0.0293	0.3819	0.1597
Daryl171	30	3.5	0	700	0	0.0258	0.4221	0.1806
Daryl172	30	3.5	0	800	0	0.0195	0.4523	0.1875
Daryl173	30	3.5	0	900	0	0.0291	0.4824	0.2153
Daryl174	30	3.5	0	1000	0	0.0441	0.5327	0.2292
Daryl175	30	3.5	6	400	0	0.0174	0.2915	0.1181
Daryl176	30	3.5	6	500	0	0.0246	0.3317	0.1389
Daryl177	30	3.5	6	600	0	0.0288	0.3719	0.1528
Daryl178	30	3.5	6	700	0	0.0232	0.4171	0.1736
Daryl179	30	3.5	6	800	0	0.0282	0.4422	0.1944
Daryl180	30	3.5	6	900	0	0.0379	0.4724	0.2083
Daryl181	30	3.5	6	1000	0	0.0398	0.5226	0.2292
Daryl182	30	3.5	8	400	0	0.0300	0.2915	0.1111
Daryl183	30	3.5	8	500	0	0.0246	0.3266	0.1389
Daryl184	30	3.5	8	600	0	0.0352	0.3719	0.1528
Daryl185	30	3.5	8	700	0	0.0286	0.4121	0.1736
Daryl186	30	3.5	8	800	0	0.0322	0.4372	0.2014
Daryl187	30	3.5	8	900	0	0.0311	0.4774	0.2153
Daryl188	30	3.5	8	1000	0	0.0354	0.5226	0.2292
Daryl189	30	3.5	10	400	0	0.0257	0.2965	0.1181
Daryl190	30	3.5	10	500	0	0.0262	0.3317	0.1319
Daryl191	30	3.5	10	600	0	0.0228	0.3769	0.1528
Daryl192	30	3.5	10	700	0	0.0281	0.4121	0.1736
Daryl193	30	3.5	10	800	0	0.0327	0.4472	0.1944
Daryl194	30	3.5	10	900	0	0.0299	0.4724	0.2083
Daryl195	30	3.5	10	1000	0	0.0417	0.5226	0.2361
Daryl196	30	2	0	400	0	0.0361	0.2944	0.1367
Daryl197	30	2	0	500	0	0.0152	0.3299	0.1511
Daryl198	30	2	0	600	0	0.0143	0.3756	0.1727
Daryl199	30	2	0	700	0	0.0279	0.4162	0.2014
Daryl200	30	2	0	800	0	0.0316	0.4569	0.2302
Daryl201	30	2	0	900	0	0.0292	0.4975	0.2302
Daryl202	30	2	0	1000	0	0.0361	0.5533	0.2590
Daryl203	30	2	6	400	0	0.0189	0.2893	0.1367

Daryl204	30	2	6	500	0	0.0358	0.3249	0.1511
Daryl205	30	2	6	600	0	0.0265	0.3756	0.1799
Daryl206	30	2	6	700	0	0.0167	0.4162	0.2086
Daryl207	30	2	6	800	0	0.0302	0.4416	0.2230
Daryl208	30	2	6	900	0	0.0289	0.4772	0.2446
Daryl209	30	2	6	1000	0	0.0273	0.5330	0.2662
Daryl210	30	2	8	400	0	0.0134	0.2893	0.1295
Daryl211	30	2	8	500	0	0.0172	0.3299	0.1655
Daryl212	30	2	8	600	0	0.0365	0.3706	0.1871
Daryl213	30	2	8	700	0	0.0291	0.4061	0.2086
Daryl214	30	2	8	800	0	0.0230	0.4467	0.2230
Daryl215	30	2	8	900	0	0.0321	0.4873	0.2374
Daryl216	30	2	8	1000	0	0.0320	0.5228	0.2662
Daryl217	30	2	10	400	0	0.0330	0.2893	0.1439
Daryl218	30	2	10	500	0	0.0200	0.3299	0.1583
Daryl219	30	2	10	600	0	0.0287	0.3756	0.1799
Daryl220	30	2	10	700	0	0.0312	0.4162	0.2014
Daryl221	30	2	10	800	0	0.0275	0.4518	0.2302
Daryl222	30	2	10	900	0	0.0304	0.4772	0.2446
Daryl223	30	2	10	1000	0	0.0380	0.5330	0.2662

C. Stochastic Gradient Descent Algorithm

```
clear all
close all


% data import
table_all = readtable('All_Results.xlsx','sheet','Quant_process');
table_Hart = table_all(1:19,:);
table_Daryl = table_all(20:end,:);
array_all = table2array(table_all(:,2:end));
array_Hart = table2array(table_Hart(:,2:end));
array_Daryl = table2array(table_Daryl(:,2:end));

% choose data subset to use
array = array_all;

% columns
width_mm = array(:,1);
theta_degs = array(:,2);
radius_mm = array(:,3);
flow_mls = array(:,4);
walls = array(:,5);
trans_m = array(:,6);
hmat = array(:,7);
hmatinf = array(:,8);

% physical constants
hmax = 0.15;
mu = 10^(-6);
rho = 10^(3);
g = 9.81;

% derived quantities
width_m = width_mm * 10^(-3); %w
theta_rads = theta_degs *(pi/180); %\theta
radius_m = radius_mm * 10^(-3); %r
```

```
flow_m3s = flow_mls * 10^(-6); %Q
walls = walls;
trans_m = trans_m; %L_{t,measured}
h0_m = hmat * hmax; %h_{0,measured}
hinf_m = hmatinf * hmax; %h_{\infty,measured}

u0_m2s = flow_m3s ./(width_m .* h0_m); %u_0
uinf_m2s = flow_m3s ./(width_m .* hinf_m); %u_\infty

% DIMENSIONLESS QUANTITIES
% PBJ's dimensionless quanitities
Fr_pbj = u0_m2s.^3 .* width_m ./ (g .* flow_m3s);
w_star = 1 + width_m ./ (2*h0_m);



% calculate L_trans_theoretical
q = hinf_m ./ h0_m;
C_D_est = q.^3 .* w_star * 2 .* sin(theta_rads) ./ Fr_pbj;
p = (2 .* Fr_pbj ./ cos(theta_rads)).^(1/3);
yinf = q;
y0 = 1;
yT = 1.05*yinf;
x_starT = 2 * sin(theta_rads) .* ...
    (...
    yT + (p.^3 - q.^3)./(6*q.^2).* ...
    (...
    -2 .* log(yT - q) ...
    + log(yT.^2 + q.*yT + q.^2) ...
    + 2*sqrt(3)*atan((2*yT + q)./(sqrt(3) * q.^2))));
x_star0 = 2 * sin(theta_rads) .* ...
    (...
    y0 + (p.^3 - q.^3)./(6*q.^2).* ...
    (...
    -2 .* log(y0 - q) ...
    + log(y0.^2 + q.*y0 + q.^2) ...
    + 2*sqrt(3)*atan((2*y0 + q)./(sqrt(3) * q.^2))));
L_starT = x_starT - x_star0;
L_trans_theoretical = h0_m .* L_starT;

% other dimensionless quantities
Re_a = (rho/mu) .* u0_m2s .* h0_m;
Fr_a = u0_m2s ./sqrt(g * trans_m);

length_ratio_a = (radius_m + width_m) ./ h0_m;
length_ratio_b = trans_m ./ h0_m;
length_ratio_c = trans_m ./ width_m;
```

```
length_ratio_d = h0_m ./ hinf_m;
% theta_rads = theta_rads;
slope = sin(theta_rads);
walls = walls;

% define response function
y = length_ratio_c;

% define predictors
x1 = Re_a;
x2 = Fr_pbj;
x3 = w_star;
x4 = slope;
x5 = walls + 1;
x6 = 2*(slope.^0); %to scale linearly
x7 = 2*(slope.^0); %to scale linearly
x8 = length_ratio_a;
x9 = length_ratio_d;

x = [x1, x2, x3, x4, x5, x6, x7, x8, x9];

% initialise exponents
n(1) = 0.0418;
n(2) = -1.0018;
n(3) = -0.7880;
n(4) = -0.0008;
n(5) = 0.1465;
n(6) = -1.3487;
n(7) = -0.6748;
n(8) = 1;
n(9) = 1;

% iterations = 10;
iterations = 10^7;
% incrementsd1 = 0.0000001;
incrementsd1 = 0.01;
decay = 1/30000;
err(1) = 1;
err(2) = 1;
for j = 3:iterations
    incrementsd = incrementsd1 * exp(-j*decay);
    y_hat = (x(:,9).^n(9)).*(x(:,8).^n(8)) .* (x(:,1).^n(1)) .*
        ↪ (x(:,2).^n(2)) .* (x(:,3).^n(3)) .* (x(:,4).^n(4)) .*
        ↪ (x(:,5).^n(5)) .* (x(:,6).^n(6))-(x(:,7).^n(7));
    absepsilon = abs(y_hat-y);
    sumabsepsilon = sum(absepsilon);
    for i = 1:length(n)
```

```
        increment = randn*incrementsd;
        n(i) = n(i) + increment;
        y_hatstar = (x(:,9).^n(9)) .* (x(:,8).^n(8)) .*
            ↪ (x(:,1).^n(1)) .* (x(:,2).^n(2)) .* (x(:,3).^n(3)) .*
            ↪ (x(:,4).^n(4)) .* (x(:,5).^n(5)) .*
            ↪ (x(:,6).^n(6))-(x(:,7).^n(7));
        absepsilonstar = abs(y_hatstar-y);
        sumabsepsilonstar = sum(absepsilonstar);
        if sumabsepsilonstar > sumabsepsilon
            n(i) = n(i) - 2*increment;
            y_hatstar = (x(:,9).^n(9)) .* (x(:,8).^n(8)) .*
                ↪ (x(:,1).^n(1)) .* (x(:,2).^n(2)) .* (x(:,3).^n(3))
                ↪ .* (x(:,4).^n(4)) .* (x(:,5).^n(5)) .*
                ↪ (x(:,6).^n(6))-(x(:,7).^n(7));
            absepsilonstar = abs(y_hatstar-y);
            sumabsepsilonstar = sum(absepsilonstar);
        end
    end
    err(j) = sumabsepsilon;
    if j == 10 || j == 10^2 || j == 5*10^2 || j == 10^3 || j ==
        ↪ 10^4 || j == 5*10^4|| j == 10^5 || j == 10^6 || j == 10^7
        figure %PLOT Response and learning at the above times ^
        fitty = fitlm(y, y_hat);
        RsquaredA = fitty.Rsquared.Adjusted;
        RsquaredO = fitty.Rsquared.Ordinary;
        x0=10;
        y0=10;
        width=1100;
        height=400;
        set(gcf,'position',[x0,y0,width,height])
        subplot(1,2,1)
        plot(log(err(ceil((length(err)/50)):end)))
        % plot(log(err), 'k')
        ylabel('Log  (Total Error)')
        xlabel('Iteration')
        title(['Iterations = ', num2str(j)])
        subplot(1,2,2)
        % For array_all
        scatter(y(1:19),y_hat(1:19), 'b', '.')
        hold on
        scatter(y(19:end),y_hat(19:end), 'r', '.')
        % For array_Daryl
        % scatter(y,y_hat, 'r', '.')
        %
        ylabel('Response')
        xlabel('Predictor')
        title(['R^2 = ', num2str(RsquaredO)])
```

```
        legend('Hart␣Data', 'Pay␣Data')
        saveas(gcf,['All_Data_', 'It_', num2str(j), '.png'])
        pause(0.001)
    end
    j
end

%% Model Consolidation (Equation vs. Experiment)
% hold off
% figure
% scatter(L_trans_theoretical, y_hat .*width_m, 'r', '+')
% hold on
% scatter(L_trans_theoretical, trans_m, 'b', '.')
% lsline
% xlabel('Theoretical Transition Length (m)')
% legend('Modelled Transition Length (m)', 'Measured Transition
    ↪ Length (m)')
```